



Rapid attribution of the August 2016 flood-inducing extreme precipitation in south Louisiana to climate change

Karin van der Wiel^{1,2}, Sarah B. Kapnick², Geert Jan van Oldenborgh³, Kirien Whan³, Sjoukje Philip³, Gabriel A. Vecchi², Roop K. Singh⁴, Julie Arrighi⁴, Heidi Cullen⁵

¹Program in Atmospheric and Oceanic Sciences, Princeton University, Princeton, U.S.

²Geophysical Fluid Dynamics Laboratory (GFDL), National Oceanic and Atmospheric Administration, Princeton, U.S.

³Royal Netherlands Meteorological Institute (KNMI), De Bilt, Netherlands

⁴Red Cross Red Crescent Climate Centre, The Hague, Netherlands

⁵Climate Central, Princeton, U.S.

Correspondence to: Karin van der Wiel (kwiel@princeton.edu) or Geert Jan van Oldenborgh (oldenborgh@knmi.nl).

Abstract.

A stationary low pressure system and elevated levels of precipitable water provided a nearly continuous source of precipitation over Louisiana, United States (U.S.) starting around 10 August, 2016. Precipitation was heaviest in the region broadly encompassing the city of Baton Rouge, with a three-day maximum found at a station in Livingston, LA (east of Baton Rouge) from 12–14 August, 2016 (648.3 mm, 25.5 inches). The intense precipitation was followed by inland flash flooding and river flooding and in subsequent days produced additional backwater flooding. On 16 August, Louisiana officials reported that 30,000 people had been rescued, nearly 10,600 people had slept in shelters on the night of 14 August, and at least 60,600 homes had been impacted to varying degrees. As of 17 August, the floods were reported to have killed at least thirteen people. As the disaster was unfolding, the Red Cross called the flooding the worst natural disaster in the U.S. since Super Storm Sandy made landfall in New Jersey on 24 October, 2012. Before the floodwaters had receded, the media began questioning whether this extreme event was caused by anthropogenic climate change. To provide the necessary analysis to understand the potential role of anthropogenic climate change, a rapid attribution analysis was launched in real-time using the best readily available observational data and high-resolution global climate model simulations.

The objective of this study is to show the possibility of performing rapid attribution studies when both observational and model data, and analysis methods are readily available upon the start. It is the authors aspiration that the results be used to guide further studies of the devastating precipitation and flooding event. Here we present a first estimate of how anthropogenic climate change has affected the likelihood of a comparable extreme precipitation event in the Central U.S. Gulf Coast. While the flooding event of interest triggering this study occurred in south Louisiana, for the purposes of our analysis, we have defined an extreme precipitation event by taking the spatial maximum of annual 3-day inland maximum precipitation over the region: 29–31 °N, 85–95 °W, which we refer to as the Central U.S. Gulf Coast. Using observational data, we find that the observed local return time of the 12-14 August precipitation event in 2016 is about 550 years (95%

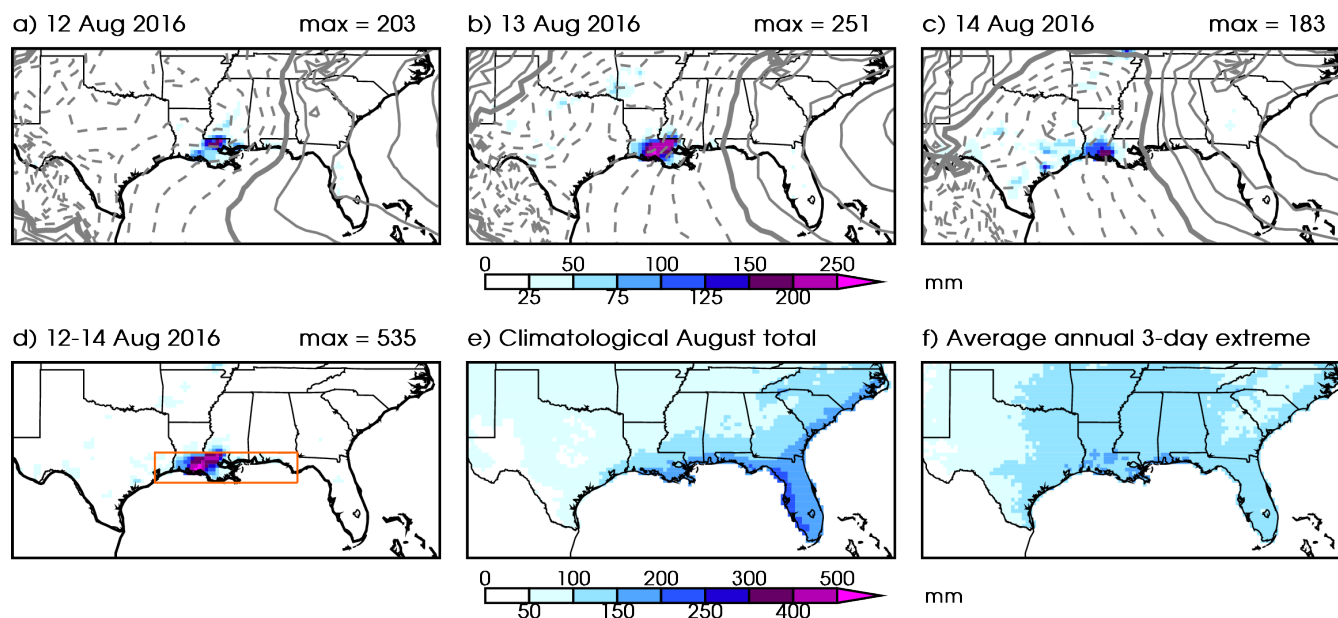


32 confidence interval (C.I.): 450-1450). The probability for an event like this to happen anywhere in the region is presently 1
33 in 30 years (C.I. 11-110). We estimate that these probabilities and the intensity of extreme precipitation events of this return
34 time have increased since 1900. A Central U.S. Gulf Coast extreme precipitation event has effectively become more likely in
35 2016 than it was in 1900. The global climate models tell a similar story, with the regional probability of 3-day extreme
36 precipitation increasing due to anthropogenic climate change by more than a factor 1.4 in the most accurate analyses. The
37 magnitude of the shift in probabilities is greater in the 25 km (higher resolution) climate model than in the 50 km model. The
38 evidence for a relation to El Niño half a year earlier is equivocal, with some analyses showing a positive connection and
39 others none.

40 **1 Introduction**

41 In the second week of August, a storm system developed in the United States (U.S.) Gulf Coast region and resulted in
42 intense precipitation across south Louisiana in the region surrounding the city of Baton Rouge. The highest concentration of
43 precipitation fell over the 3-day period of 12-14 August (Figure 1a-d). Saturday, 13 August experienced the greatest total
44 magnitude of precipitation and the broadest surface area of intense precipitation during the storm. The National Oceanic and
45 Atmospheric Administration (NOAA) Climate Prediction Center (CPC) unified gauge-based gridded analysis of daily
46 precipitation exhibits 25×25 km area boxes with precipitation maxima reaching up to 534.7 mm (21.1 inches) over the 3-day
47 period. In station observations (a single point), a rain gauge in Livingston, LA (east of Baton Rouge) experienced an even
48 higher 3-day precipitation total of 648.3 mm (25.5 inches). In places, the 3-day precipitation totals in Louisiana exceeded
49 three times that of the climatological August totals (historical average total precipitation that occurs over 31-days, Figure 1e)
50 and three times the average annual 3-day precipitation maximum (Figure 1f).

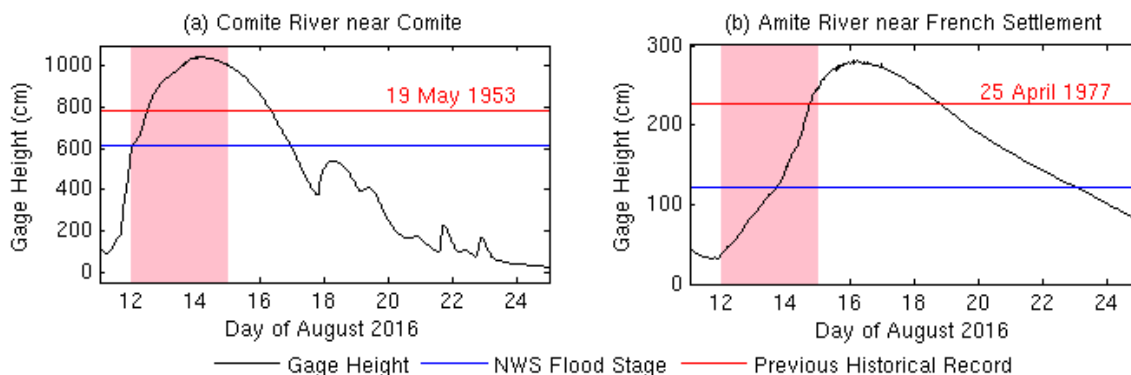
51 The intense precipitation formed due to a low pressure system that originated near Florida/Alabama on 5 August. At
52 that time the National Hurricane Center stated that it might transform into a tropical depression after moving to the Gulf of
53 Mexico (Schleifstein 2016). Instead the system remained over land and moved westward slowly. On 12 August it became
54 near-stationary over Louisiana (Figure 1a-c) allowing for the continuous development of thunderstorms in localized area to
55 the south and southeast of the low pressure center. The stationary storm system and anomalously moist atmospheric
56 conditions (precipitable water exceeding 65 mm) created optimal conditions for high precipitation efficiencies and intense
57 precipitation rates. Though the system had a warm-core and some similarities to a tropical depression, it never formed the
58 closed surface wind circulation about a well-defined center that are needed to be classified as one (National Weather Service
59 2016).



60

61 **Figure 1:** (a,b,c) Daily precipitation (shaded colors) and sea level pressure (grey contours, interval 1 hPa, 1015 hPa contour
62 thickened, lower contours dashed) for 12, 13 and 14 August, 2016. (d) 3-day precipitation sum 12-14 August, 2016. (e)
63 August climatological total precipitation (1948-2015). (f) Average annual maximum 3-day precipitation event (1948-2015).
64 Orange box in (d) shows the geographic region used for the analysis (29°-31°N, 85°-95°W). Data from CPC unified gauge-
65 based analysis of daily precipitation over the contiguous U.S. (2016 data from the real time archive) and ECMWF
66 operational analysis.

67 Historic freshwater flooding in the region encompassing Baton Rouge, Louisiana followed the extreme precipitation
68 event. Provisional reports from 18 August, 2016 showed streamgauges managed by the United States Geological Survey
69 (USGS) registering above flood stage levels at 30 sites and found that out of 261 sites in all of Louisiana 50 were overtopped
70 by floodwaters (Burton and Demas 2016). This was a complex event where provisional data from the USGS showed rivers
71 responding to local precipitation as well as upstream and downstream conditions (Figure 2). For example, on the Comite
72 River, a major drainage river for North Baton Rouge and its outlying districts, the provisional gauge height data exceeded
73 the National Weather Service (NWS) flood stage from 12-16 August and even exceeded the previous height record (set 19
74 May, 1953). The Comite River hit its NWS flood stage level before the maximum precipitation fell in Central U.S. Gulf
75 Coast (Figure 1d). Floodwaters were slow to recede due to flood stages downstream causing backwater flooding (upstream
76 flooding caused by conditions downstream) in many neighborhoods (Burton and Demas 2016). Further downstream on the
77 Amite River, provisional data showed that water levels exceeded the NWS floodstage from 13-23 August and also exceeded
78 the previous height record (set 25 April, 1977). Its levels declined more slowly and did not fall below floodstage until late on
79 23 August, due to drainage from the Comite and other tributaries upstream that hit peak floodstage days earlier (Burton and
80 Demas 2016).



81

82 **Figure 2:** Hydrographs of gauge levels, NWS flood stage value and previous historical record for USGS station (a)
83 07378000 on the Comite River and (b) 07380200 on the Amite River. Observed streamgauge information downloaded 25
84 August, 2016 from the USGS: <<http://waterdata.usgs.gov/la/nwis/uv?>>; provisional USGS data is subject to adjustment:
85 <http://help.waterdata.usgs.gov/policies/provisional-data-statement>.

86 On 12 August the NWS issued flash flood warnings for parishes in south Louisiana, and activated the national
87 Emergency Alert System which urged residents to move to higher ground. The Louisiana Coast Guard, National Guard, and
88 civilian volunteers mobilized to rescue over 30,000 people from their flooded homes and cars (Broach 2016). By August 14,
89 the federal government declared a major disaster, indicating that the severity of damage exceeded the local and state
90 governments' combined capability to respond, initiating federal assistance for individuals and public infrastructure (Davies
91 2016, FEMA 2016, Stafford Disaster Relief and Emergency Assistance Act). The flooding impacted the state's agriculture
92 industry with losses estimated in excess of \$110 million (Allen and Burgess 2016). Initial estimates also show that at least
93 60,600 homes were damaged, and thirteen people were killed due to the floods (Strum 2016). The American Red Cross, with
94 FEMA and other federal and local agencies, provided shelter and emergency relief for 10,600 people initially displaced by
95 the disaster, and the American Red Cross estimates that its ongoing relief efforts will cost \$30 million (American Red Cross
96 2016). To date, more than 110,000 people have registered for federal disaster assistance (FEMA, 2016). FEMA has made
97 grants totalling \$107 million available to disaster survivors for serious needs including temporary rental assistance, and \$20
98 million in advance payments for National Flood Insurance policyholders (FEMA 2016).

99 South Louisiana is a region where a number of phenomena can lead to flooding. For example, as a coastal region, it
100 can experience saltwater flooding from a storm surge, when the low pressure and winds of a storm moving towards the
101 coastline push coastal saltwater inland. This occurred in August 2005 when Hurricane Katrina impacted a broad swath of the
102 Gulf Coast, including New Orleans, LA, with a large storm surge. Inland, precipitation can directly cause pluvial flooding by
103 producing runoff in a region independent of a body of water (i.e. when more rain falls than can be soaked up by the ground)
104 or fluvial flooding when water levels exceed the capacity of the river environment. For inland freshwater flooding, land
105 surface conditions prior to an extreme precipitation event may increase the susceptibility of a region to both types of
106 flooding, by saturating the soil (Tramblay et al. 2010, De Michele and Salvadori 2002) or increasing river levels (Pinter



107 2006). Inland flood conditions can also be induced by water flowing through the river system after a storm due to capacity
108 limitations, as evident along the Amite River in August 2016 (Figure 2b) due to upstream flood conditions making their way
109 downstream. Flooding can be influenced by remote meteorological conditions as river networks connect regions over vast
110 areas. Louisiana had most recently experienced widespread inland flooding in March-April 2016. Although inland
111 freshwater flooding occurs due to a combination of the level of extreme precipitation and its interaction with the land surface
112 and river system, including human modifications to those systems and responses to events, we have chosen to focus our
113 rapid attribution study on one portion of the problem: understanding the present and potentially climate change-influenced
114 probability of extreme precipitation events like the one which occurred in August 2016.

115 Synoptic forcing for precipitation extremes in the Gulf Coast region includes both mid-latitude weather (cold core
116 systems fueled by baroclinic instability), and tropical weather (warm core systems with barotropic instability). Extreme
117 precipitation has historically been classified into 3 types of events: frontal systems, tropical systems, and air mass events.
118 Each of these categories can be further broken down; e.g. tropical systems ranging from easterly waves to hurricanes, frontal
119 systems including interactions between the polar jet and moist air masses from the Gulf, squall lines, or mesoscale
120 convective systems, and air mass systems that may include heavy rainfall from upper air disturbances, or convective storms
121 that form because of daytime heating (Keim and Faiers 1996). The variety of weather systems that can give rise to
122 precipitation extremes in the region complicates the statistical analysis of the extremes and requires climate models to
123 capture the entire distribution in a realistic manner. Also, the response to radiative forcing may be non-linear:
124 thermodynamic and/or dynamic changes may be different for each weather type.

125 In this article, we analyze the historical context and changes in statistics of extreme precipitation like the one
126 experienced during August 2016 in south Louisiana by defining an extreme event by its local or regional maximum 3-day
127 precipitation. We have focused our analysis on stations or land surface grid cells in the region: 29–31 °N, 85–95 °W
128 (illustrated by the red box in Figure 1d), which we hereafter refer to as the “Central U.S. Gulf Coast”. Here we report the
129 results of our rapid attribution study conducted by several organizations within two weeks of the event. The need for a rapid
130 attribution study arises from the current intense public discussion that results from the significant societal impacts of this
131 particular event and a continuous general interest in climate change. Media coverage following the event has linked into the
132 growing body of scientific evidence that precipitation extremes are expected to increase due to the greater moisture content
133 of a warmer atmosphere following Clausius-Clapeyron scaling (O’Gorman 2015, Lenderink and Attema 2015, Scherrer et al,
134 2016): e.g. “Disasters like Louisiana floods will worsen as planet warms, scientists warn” (Milman 2016), “Flooding in the
135 South looks a lot like climate change” (Bromwich 2016). However, specific scientific statements for the event as observed in
136 south Louisiana cannot be made based on general assessments of the connection of global warming and extreme rainfall.
137 While attribution studies at a more traditional scientific pace (several months up to a year later) are important and add to
138 scientific understanding of changing extremes, reporting results recently after an extreme event may enhance the societal



139 understanding of climate change and extreme weather, and provide often requested information for management decisions
140 following the event.

141 The methodologies employed in this study are used regularly in the literature and were previously applied to the
142 rapid attribution of the French and German 2016 flooding event (Van Oldenborgh et al. 2016) and of Storm Desmond over
143 the UK in 2015 (Van Oldenborgh et al. 2015). The presented analysis builds upon these methodologies for anthropogenic
144 climate change attribution and also explores the role of climate variability. The trends and internal climate variability of
145 extreme precipitation is investigated in station observations, gridded gauge-based precipitation analysis, and high-resolution
146 global climate model simulations. Since this paper aims to provide a first attribution assessment of the 2016 south Louisiana
147 extreme event, we have provided a detailed data and methods section (Section 2) in which our data sets, statistical
148 calculations for return periods and trends and data set validation methodologies are described. The rest of the paper is
149 organized as follows: Section 3 provides observational analysis. In Section 4 we evaluate the suitability of the global climate
150 models. Model analysis is provided in Section 5. Section 6 synthesizes our conclusions. In Section 7 we provide a detailed
151 discussion of crucial assumptions and their potential impact on the results, further avenues of research and implications of
152 this work.

153 **2 Data and methods**

154 **2.1 Observational data**

155 We utilize both point station observations and gridded analysis in this paper. The point station data are from the Global
156 Historical Climatology Network daily product (GHCN-D) version 3.22 (Menne et al. 2012, 2016). The data set provides
157 daily observations for stations worldwide. Data is quality controlled before becoming available in near-real time. Inside the
158 defined Central U.S. Gulf Coast (Figure 1d), 324 stations with a minimum of 10 years of data are available for the period
159 1891 to present (August 2016). However, not all stations provide data for the entire period, and spatial proximity between
160 stations means that not all data points provide independent information. Therefore for some analyses a smaller selection of
161 the available stations is taken into account. Selection criteria are described in the relevant sections.

162 The gridded analysis used here is the product of the NOAA Climate Prediction Center (CPC) Unified Gauge-Based
163 Analysis of Daily Precipitation over the contiguous U.S. (Higgins et al. 2000). The data set interpolates point station data on
164 a $0.25^{\circ} \times 0.25^{\circ}$ uniform latitude-longitude grid, based on the optimal interpolation scheme of Gandin and Hardin (1965). The
165 CPC dataset covers the period 1 January 1948 to present (August 2016), data from 2007 onwards has been made available in
166 real time. Because this is a gridded product, daily precipitation sums represent an areal average ($0.25^{\circ} \times 0.25^{\circ}$) rather than a
167 point measurement. Therefore precipitation extremes are expected to be of smaller magnitude in the gridded product (Chen
168 and Knutson 2008), as was noted for the south Louisiana event above (3-day total maxima of 534.7 mm in the CPC gridded
169 versus 648.3 mm in the point station data). The gridded analysis and the individual station data are not independent, as the



170 precipitation station data is the underlying source for the gridded analysis; consequently, changes in gauge station density in
171 space and time (as discussed above for GHCN-D) also impact the gridded analysis. We note that, for comparisons with
172 climate models - in which precipitation represents area averages, and not point values - the area-averaged precipitation
173 values from the gridded analysis are likely more meaningful for comparison with models than point station data (Chen and
174 Knutson 2008, Eggert et al, 2015).

175 We use the National Aeronautics and Space Administration (NASA) Goddard Institute for Space Science (GISS)
176 surface temperature analysis (GISTEMP, Hansen et al. 2010) for estimates of the development of global mean surface
177 temperature over time. This gridded data set is based on the GHCN point station data over land, NOAA Extended
178 Reconstructed Sea Surface Temperature (ERSST, Huang et al. 2015) version 4 over oceans and Scientific Committee on
179 Antarctic Research (SCAR) point station data for Antarctica.

180 **2.2 Model and experiment descriptions**

181 Many of the meteorological phenomena that cause extreme precipitation at the U.S. Gulf Coast are small-scale, therefore
182 only high-resolution models can simulate them realistically. We verified that the Royal Netherlands Meteorological Institute
183 (KNMI) EC-Earth 2.3 T159 experiments (~150km, Hazeleger et al. 2012) and the United Kingdom (U.K.) Met Office
184 HadGEM3-A N216 (~60km, Christidis et al. 2013) models do not realistically represent precipitation extremes in the region.

185 We therefore use two higher-resolution global climate models in our analysis from the NOAA Geophysical Fluid
186 Dynamics Laboratory (GFDL). Both models were developed from the GFDL Coupled Model version 2.1 (CM2.1, Delworth
187 et al. 2006) using a cubed-sphere finite volume dynamical core (Putman and Lin 2007) with 32 vertical levels. Atmospheric
188 physics are taken from the GFDL Coupled Model version 2.5 (CM2.5, Delworth et al. 2006, 2012). The two models share
189 the same ocean and sea ice components with a 1° horizontal resolution, but differ in their atmosphere and land horizontal
190 resolution. In the Forecast-oriented Low Ocean Resolution model (FLOR, Vecchi et al. 2014), there are 180 points along
191 each cubed-sphere finite volume dynamical core face (FV3-C180), which relates to a resolution of 0.5° per cell along the
192 Equator. This has been interpolated to a 0.5°×0.5° uniform latitude-longitude grid. In the high-resolution version of the
193 model (HiFLOR, Murakami et al. 2016), there are 384 points along each face (FV3-C384) on the cubed-sphere finite volume
194 dynamic core, which relates to a resolution of 0.23° per cell along the Equator. This has been interpolated to a 0.25°×0.25°
195 uniform latitude-longitude grid. For FLOR we use a flux-adjusted version of the model (FLOR-FA), in which atmosphere-
196 to-ocean fluxes of momentum, enthalpy and freshwater are adjusted to bring the simulated fields closer to their observed
197 climatological state. The adjustment method is described in detail in Vecchi et al. (2014). Descriptions on how to access the
198 data used in this study are provided in the Data Availability section.

199 Table 1 describes six different global coupled model experiments that have been performed using FLOR-FA and
200 HiFLOR, which —for each model— differ in the type of radiative forcing that is prescribed, thus allowing us to assess the
201 impact of radiative forcing on the statistics of weather extremes in these models. With FLOR-FA there are two sets of



202 experiments. First, we made use of a multi-centennial integration in which values of radiative forcing agents (solar forcing,
 203 anthropogenic and natural aerosols, well-mixed greenhouse gases, ozone, etc.) are prescribed to remain at levels
 204 representative of a particular time - the mid-19th century in this case (Jia et al. 2016); radiative forcing agents are prescribed
 205 at the 1860 values following the protocol of the Fifth Coupled Model Intercomparison Project (CMIP5, Taylor et al. 2009).
 206 These types of experiments with global climate models are often referred to as “control” experiments (“pre-industrial
 207 control” in this particular case) but here we label this class of experiments as “static radiative forcing” experiments, since
 208 with HiFLOR we fix radiative forcing at a number of levels. In the static radiative forcing experiments the years of the
 209 integration bear no relation to the real world calendar. The second set of experiments with FLOR-FA is a suite of five
 210 realizations (or “ensemble members”) in which the radiative forcing is prescribed to follow estimates of past and future
 211 radiative forcing changes over the period 1861-2100 (Jia et al. 2016); the forcing agents for the period 1861-2005 are
 212 prescribed to follow the CMIP5 historical experiment protocol, and for the period 2005-2100 they follow the CMIP5
 213 Representative Concentration Pathway 4.5 (RCP4.5), which represents the medium range greenhouse gas emissions scenario
 214 (Van Vuuren et al. 2011). The five realizations of 1861-2100 experiments differ only in their initial conditions on January 1,
 215 1861, which are taken from five different years from the long FLOR-FA preindustrial static forcing experiment. In these
 216 experiments, the calendar of the experiments is connected to the history of radiative forcing - but the internal climate
 217 variations (e.g., El Niño events) and weather fluctuations (e.g., individual storms) are not constrained to follow their
 218 observed sequence. The static climate experiment has a slow drift because the slow climate components, notably the deep
 219 ocean, were not in equilibrium at the beginning of the run, this is most noticeable in the first 1000 years of the integration.

220

221 **Table 1:** Global coupled model experiments performed with the FLOR-FA and HiFLOR models.

Model	Type of forcing	Representative year of forcings	No. of ensembles	No. of modeled years in total
FLOR-FA	Static radiative forcing	1860	1	3550
FLOR-FA	Time-varying radiative forcing	1861-2100	5	1200 (5 realizations of 240 years)
HiFLOR	Static radiative forcing	1860	1	200
HiFLOR	Static radiative forcing	1940	1	75
HiFLOR	Static radiative forcing	1990	1	300
HiFLOR	Static radiative forcing	2015	1	70

222

223 With HiFLOR, there are four experiments to explore the climate sensitivity of the statistics of weather events
 224 through static radiative forcing experiments at levels representative of particular times: preindustrial conditions (fixed at
 225 1860 values), mid-20th Century (fixed at 1940 values), late-20th Century (fixed at 1990 values), and early 21st Century (fixed
 226 at 2015 values). The value of radiative forcing agents in these experiments is prescribed from either the CMIP5 Historical
 227 Forcing protocol (for the 1860, 1940 and 1990 static forcing experiments) or from the CMIP5 RCP4.5 protocol (for the 2015
 228 static forcing experiment); and the coupled atmosphere-land-ocean-sea ice state of the model is left to evolve freely. These
 229 simulations have been integrated for different lengths of time (Table 1, last column), over which they generate their own



230 climate under the fixed forcing; longer integrations allow us to better estimate the statistics of climate extremes, but these
 231 were the lengths of integrations available as of 15 August, 2016.

232 There are many fewer model years available with HiFLOR than FLOR-FA because the HiFLOR model was
 233 developed more recently, and because the HiFLOR model is substantially more computationally intensive (~6× the computer
 234 resources required for one year of integration) than FLOR-FA. The four HiFLOR static forcing experiments are initialized
 235 from the same ocean, atmosphere, land and sea ice initial conditions, which are representative of the observed state in the
 236 late 20th century, and the four experiments are not in radiative balance through the length of integration (the 1860
 237 experiment has a negative top of atmosphere balance, while the 1940, 1990 and 2015 experiments have positive balances).
 238 Therefore these static climate experiments each exhibit an initial rapid (~20 year) adjustment away from the late-20th
 239 century observed initial conditions, and a slower climate drift reflecting the top of atmosphere imbalance over the length of
 240 the integration. We exclude the first twenty years of each integration from our analysis, and assume (see Section 7.1) that the
 241 impact of the slow climate drift in each model experiment on the statistics of precipitation extremes is small.

242 In addition to the coupled model experiments discussed above, in which the history of sea surface temperatures
 243 (SSTs) in the models emerges from the dynamics of the models and the changes in radiative forcing, for HiFLOR a set of
 244 variable forcing experiments were run over 1971-2015 in which the model is constrained by both historical radiative forcing
 245 and the observed history of monthly SST (Table 2). These experiments can be used to connect the statistics of rainfall
 246 extremes to the detailed history of SSTs that occurred over the past 45 years, part of which was a response to radiative
 247 forcing changes and part of which emerged from internal climate variations. Furthermore by construction, these experiments
 248 have a substantially smaller SST bias than the free running versions of HiFLOR, as the statistics of weather extremes and
 249 their connection to larger-scale climate can be substantially affected by SST biases (e.g. Vecchi et al. 2014; Krishnamurthy
 250 et al. 2015; Pascale et al. 2016). These experiments are described in more detail in Murakami et al. (2015) and Van der Wiel
 251 et al. (2016). The model SST was restored to the interannually varying observed field (SST_{τ}) Met Office Hadley Centre SST
 252 product (HadISST1.1, Rayner et al. 2003) by adding an extra term to to the modeled SST tendency:

$$253 \quad \frac{dSST}{dt} = O + \frac{1}{\tau}(SST_{\tau} - SST) \quad \text{Eq. (1)}$$

254 with τ the restoring time scale (three ensemble members were produced with $\tau = 5$ days, three with $\tau = 10$ days).

255

256 **Table 2:** Restored SST experiments performed with the HiFLOR model.

Model	Type of forcing	Representative year of forcings	No. of ensembles	No. of modeled years in total
HiFLOR	Time-varying radiative forcing agents (CMIP5 Historical and RCP4.5); SSTs restored to observed monthly observations	1971-2015	6	270 (6 realizations of 45 years)



257 2.3 Defining an extreme event and its statistics

258 To classify the August 2016 south Louisiana flooding event, we must choose a definition for the event to guide our statistical
259 analysis of observations and model experiments. We have chosen to classify extremes using multi-day averaged precipitation
260 rather than single-day precipitation, to reflect the aspects of the event that resulted in the flooding of several rivers in the
261 area. The following steps are taken to calculate our event statistics in the model and observations.

262

- 263 1. We create 3-day precipitation averages in station points/grid cells over land found in the Central U.S. Gulf Coast:
264 29–31 °N, 85–95 °W, which has relatively homogenous average precipitation extreme magnitude (Figure 1f). This
265 provides us with, for each point in space, 365 values per year (366 in leap years) for each station point/grid cell,
266 except the last and first years in the record when there are 364 values per year (365 in leap years), since the first
267 January 1 and last December 31 are dropped.
- 268 2. We then, at each point in space, calculate the annual maximum for each year and define it as the local extremum for
269 the year to create a set of extreme values for further analysis.
- 270 3. For some analyses we then take the maximum over the region. We have carefully documented in the main text
271 when this is the case.
- 272 4. In the static forcing model experiments, we disregard the first 20 years of data to allow for some initial spin-up of
273 the model in each new static forcing state.

274

275 In order to estimate the observed return periods using the 3-day annual events found above, we fit the resulting data
276 to a Generalised Extreme Value (GEV) Distribution (Coles, 2001) in a similar manner as previously done for rapid
277 attribution of the 2015 storm Desmond over the UK (Van Oldenborgh et al. 2015) and for the rapid attribution of the 2016
278 flooding in France and Germany (Van Oldenborgh et al. 2016). We first analyze the GEV distribution of observations and
279 model simulations to determine if they represent the statistics of summertime extreme precipitation events sufficiently to
280 employ them in further work. To account for possible changes due to anthropogenic climate change over time, we scale the
281 distribution with the 4-year smoothed global mean temperature (GISTEMP for observational analysis, modeled global mean
282 2m air temperature for model analysis), a measure of the uniform global climate response to forcing. The GEV function is
283 represented by:

$$284 \quad F(x) = \exp \left[- \left(1 + \xi \frac{x - \mu}{\sigma} \right)^{1/\xi} \right], \quad \text{Eq. (2)}$$
$$285 \quad \mu = \mu_0 \exp \left(\frac{\alpha T'}{\mu_0} \right),$$
$$286 \quad \sigma = \sigma_0 \exp \left(\frac{\alpha T'}{\mu_0} \right).$$

287 Where μ is the location parameter, σ is the scale parameter, and ξ represents the shape parameter of the curve. The ratio of
288 σ/μ reduces to the constant σ_0/μ_0 . The fit is estimated using a maximum likelihood method where σ , μ_0 , σ_0 and ξ are varied.



289 There is a penalty term on ξ : a Gaussian with a width of 0.2 is added to the likelihood function such that values larger than
 290 ~ 0.4 are penalized as unphysical. This is mainly used to restrain fits to the 1000-member non-parametric bootstrap that is
 291 used to estimate uncertainty. All years are assumed to be independent for this analysis, however correlations between
 292 proximate stations or ensemble members (when available) are taken into account with a moving block technique. The
 293 average number of dependent stations will be noted in the analysis.

294 The GEV is first estimated for observational data to provide a baseline for validation. We then evaluate the
 295 individual models by assessing the extent to which the GEV fit parameters (μ , σ and ξ) are similar to those fitted to the
 296 longest available observational analysis (GHCN-D). As in Van Oldenborgh et al. (2016), multiplicative bias correction is
 297 employed for the model data, which tends to improve the similarity of the GEV fit from the model and the observations.

298 After a conditional GEV fit has been computed, with global mean surface temperature as the covariate, Eq. (2) can
 299 be inverted to find the probability of the south Louisiana event in any year. We thus estimate the probability for the south
 300 Louisiana event in 2016, p_1 , and its probability in some earlier year, p_0 - taken as 1900 or the first year with available data if
 301 that is later. The year 1900 is taken as representative for a climate that has not yet been strongly influenced much by
 302 anthropogenic climate change. The probabilities for an event with a magnitude at least as great as that observed in south
 303 Louisiana in each year, i , can be expressed as return times, τ_i , by:

$$304 \quad \tau_i = 1/p_i \quad \text{Eq. (3)}$$

305 The ratio of probabilities or return periods from different years is known as the risk ratio where:

$$306 \quad RR = p_1/p_0 = \tau_0/\tau_1 \quad \text{Eq. (4)}$$

307 The risk ratio is a measure of how the likelihood of an event has changed in the target year (*e.g.*, 2016) versus a reference
 308 year (*e.g.*, 1900). A *RR* value of 1 would mean that the likelihood has not changed in the baseline year versus the target year.
 309 This ratio is therefore an indicator of changes in likelihood, but alone it cannot attribute this difference to a given
 310 mechanism.

311 There are multiple methods available to evaluate the impact of radiatively-forced climate change on the change in
 312 likelihood of events. For FLOR-FA, we repeat the analysis for the observations using data from the transient experiments.
 313 The natural variability from an ensemble member of the model is uncorrelated with that of other ensemble members, or the
 314 real world, so common changes in the ensemble members are therefore due to the prescribed external forcings. Multi-
 315 decadal changes over the past century are dominated by anthropogenic forcings. For the highest-resolution global climate
 316 model, HiFLOR, we fit a concatenated time series of maximum precipitation and the corresponding global mean
 317 temperatures from the four static forcing experiments to Eq. (2). Furthermore, in HiFLOR we fit the trends in extremes in the
 318 variable forcing 6-member ensemble covering 1971-2015. These simulations feature restored SSTs which reduce oceanic
 319 temperature biases compared to a fully free running ocean component and include the same oceanic variability as the real
 320 world (*e.g.* El Niño events, North Atlantic decadal variability).



321 We use the same procedure to investigate the effect of ENSO on extreme precipitation on the U.S. Central Gulf
322 Coast, replacing the smoothed global mean temperature by an index of the strength of El Niño as covariate in Eq. (2). As the
323 2016 flooding occurred half a year after a strong El Niño event, we take as an index a detrended version of the Niño3.4 index
324 with a lag of six months. The detrending is done by subtracting the average SST over 30 °S–30 °N.

325 **3 Observational analysis**

326 We here describe the character of the statistical distribution of observed precipitation extremes and their trends in the
327 GHCN-D point station data and the CPC gridded analysis by fitting to a time-dependent GEV distribution (described in
328 Section 2.3). Due to the many different meteorological phenomena that can lead to precipitation extremes in the Central U.S.
329 Gulf Coast, we assess the extent to which the GEV gives a satisfactory description of the underlying data. We frame the
330 results around measures of the probability per year of an event at least as intense as the 2016 south Louisiana event
331 (expressed as a return time), and the change of return time from the beginning of the dataset to present (risk ratio). These
332 return times can be assessed at a local scale (the expected wait time for an event at a particular place) or at a regional scale
333 (the expected return time for an event *somewhere* in the Central U.S. Gulf Coast). Because the spatial scale of the most
334 extreme precipitation events is substantially smaller than the whole region, the local return times are longer than the regional
335 return times. This observational analysis on its own is only able to detect whether a trend is present, but cannot ascribe
336 cause(s) to these trends. Note that from here onwards we will principally report 3-day average precipitation values rather
337 than 3-day precipitation sums, unless stated otherwise.

338 **3.1 Point station data**

339 We first analyze point station data, as extremes are affected by interpolation and station density, using the GHCN-D v3.22
340 dataset. This first analysis does not take the spatial maximum (Step 3 in Section 2.3), but analyzes all stations in the region
341 with at least 10 years of data. This gives 324 stations with 12536 station years with data (Figure 3a), though it is crucial to
342 note that they are not all statistically independent. The highest observed value at these gauges in 2016 is 216.1 mm/day at
343 Livingston, LA on 12–14 August (648.3 mm, three-day sum).

344 Fitting these data to a time-dependent GEV distribution as described in Section 2.3 gives a reasonable description of
345 the data (Figure 3c,e), although the fit is shaped mainly by the lower-intensity events and the highest-intensity events align
346 closer to the lower bound. It should be noted that for each point station in the dataset, on average another 18 are correlated
347 with $r > 1/e$, so the number of degrees of freedom is much less than the number of points. Overall it is surprising that all
348 different meteorological situations that can give rise to extreme precipitation (as laid out in Section 1) can be described with
349 a single GEV function.



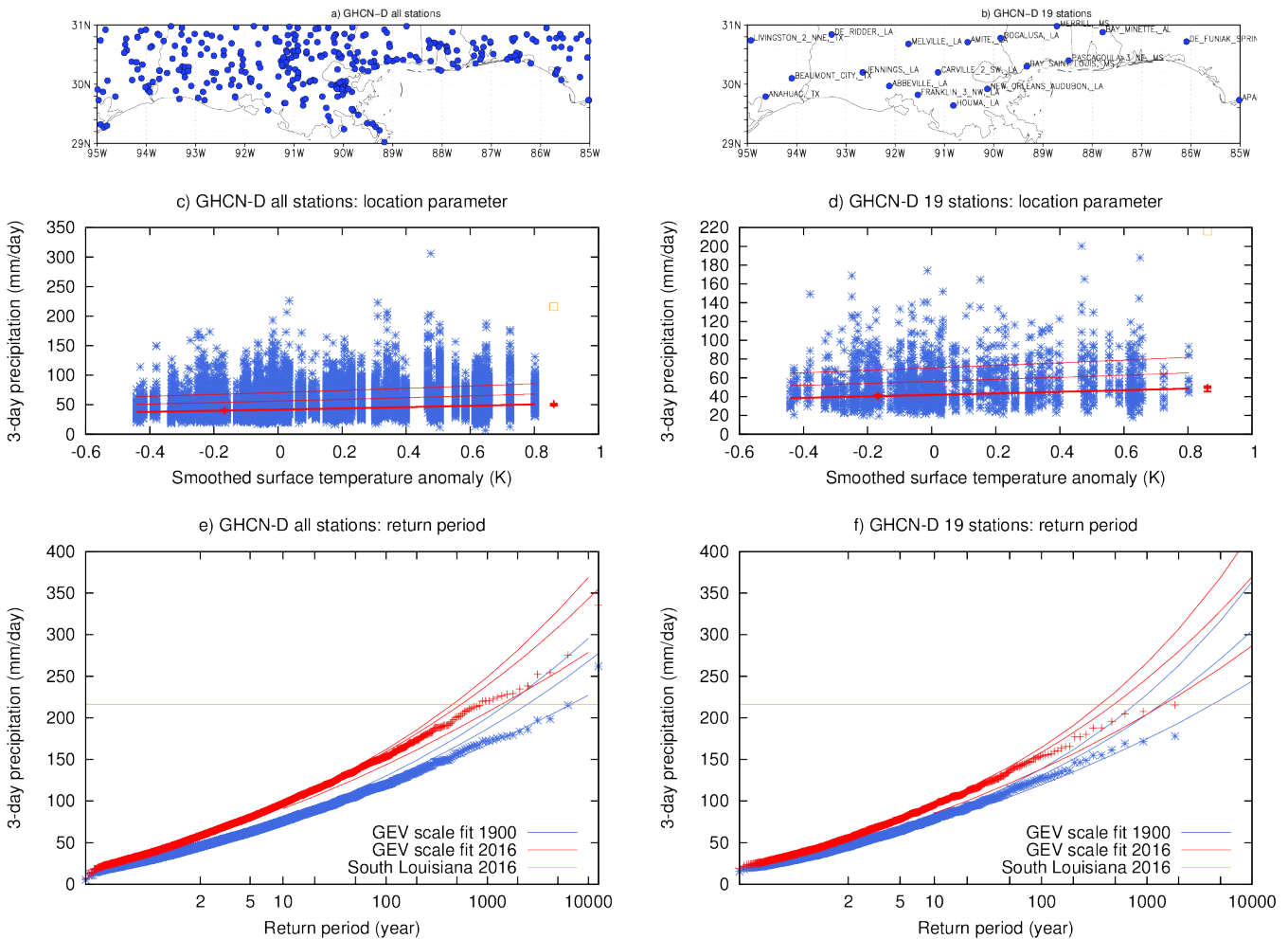
350 The local return time of a 216.1 mm/day event at a station in 2016 is about 550 yr (95% Confidence Interval, C.I.,
351 450-1450 yr). The probability of a 3-day precipitation event at a station with 216.1 mm/day or more has increased by a factor
352 4.5 (C.I. 3.0-5.5) since 1900 in this analysis. This corresponds to an increase in intensity for a given return time of 22% (C.I.
353 16%-22%).

354 This fit of all data available may be influenced by the spatially and temporally varying numbers and locations of
355 stations. We therefore evaluate the impact of these changes in sampling on the results by limiting the analysis to stations
356 with at least 80 years of data and at least 0.5° of spatial separation between stations. This leaves 19 stations with 1849 station
357 years (Figure 3b), which results in 2.3 stations per degree of freedom on average. This analysis gives similar results: a return
358 time of about 500 years (C.I. 360-1400) and an increase in probability of a factor 2.8 (C.I. 1.7-3.8), corresponding to an
359 increase in intensity of 17% (C.I. 10%-21%), Figure 1d,f. The increase in probability is less than in the full station sample,
360 although compatible within the 2σ uncertainties. As the impact of inhomogeneities is smaller when considering longer time
361 series, we use this result from the 19 GHCN-D point stations for the trend estimate.

362 Our final analysis of point station data focuses on the most intense events only by considering the spatial maximum
363 of 3-day averaged precipitation anywhere in the Central U.S. Gulf Coast (Step 3 in Section 2.3). This answers the question
364 how likely an event, like that of south Louisiana 2016 or worse, was anywhere in the region, rather than at a specific place.
365 In the point station data, the spatial maximum is only homogeneous when the number of stations does not vary by much. We
366 therefore again consider only those stations with at least 80 years of data, but do not require a minimum distance this time.
367 The number of stations increases up to around 40 in 1950–1980 and decreases again to the present. On average 1.3 stations
368 are correlated at $r > 1/e$ with each of these stations. We consider the period 1930-2016. The decrease in number of stations at
369 the end implies that a trend in extremes will be negatively biased. The number of events is lower than before (1 per year
370 instead of 19/324 events per year), so the uncertainties are larger.

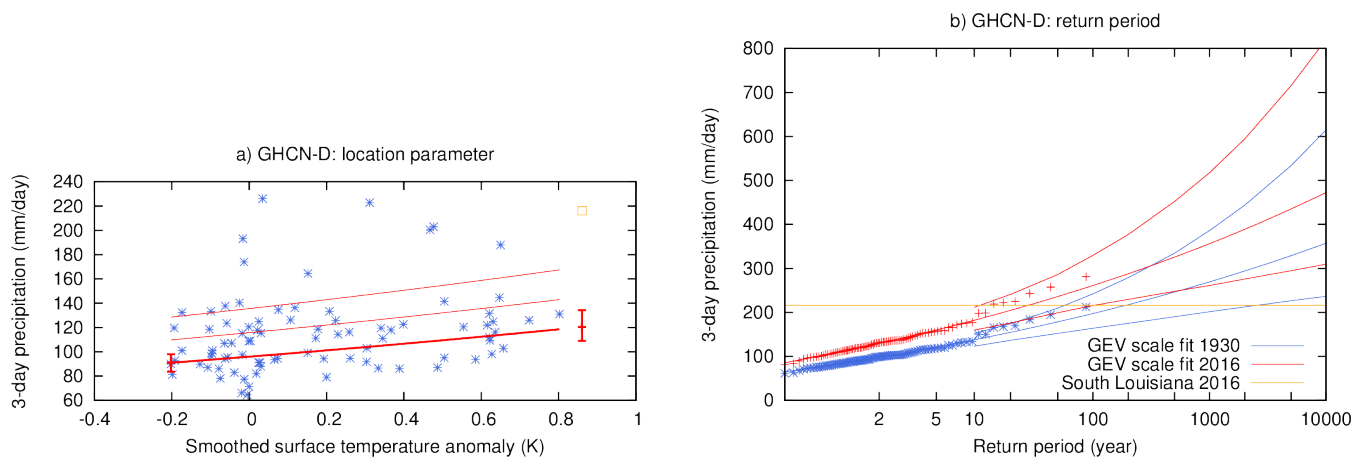
371 A fit of a time-dependent GEV to the annual and spatial maximum of 3-day averaged precipitation describes the
372 data well (Figure 4). The return time for an event like south Louisiana 2016 anywhere in the Central U.S. Gulf Coast is
373 currently around 30 yr (between 11 yr and 110 yr with 95% C.I.). This is a factor 6.3 (C.I. 2.1-50) more than it was in the
374 climate of 1930, corresponding to an increase of intensity of about 25% (C.I. 12%-35%).

375 Analyses of station data analogous to the ones above but for the season July-August-September (JAS) show
376 somewhat smaller trends, but with larger error margins. The estimated ranges of the JAS analyses and the all year analyses
377 overlap.



378

379 **Figure 3:** Fit of the annual maximum 3-day average GHCN-D station precipitation on the Central U.S. Gulf Coast to a GEV
 380 that scales with smoothed global mean surface temperature. (a) Location of all GHCN-D stations with minimum 10 years of
 381 data, (c) observations (blue marks), location parameter μ (thick red line versus global mean temperature anomalies, relative
 382 to 1980-2010), $\mu + \sigma$ and $\mu + 2\sigma$ (thin red lines), the two vertical red lines show μ and its 95% C.I. for the two climates in
 383 (e). (e) Gumbel plot of the GEV fit in 2016 (red line, with 95% uncertainty estimates) and 1900 (blue line), marks show data
 384 points drawn twice: scaled up with the trend to 2016 and scaled down to 1900. The yellow square (line) denotes the intensity
 385 of the observed event at Livingston, LA. (b,d,f) as (a,c,e) but for 19 GHCN-D stations with minimum 80 years of data and
 386 minimum spatial separation of 0.5°.



387

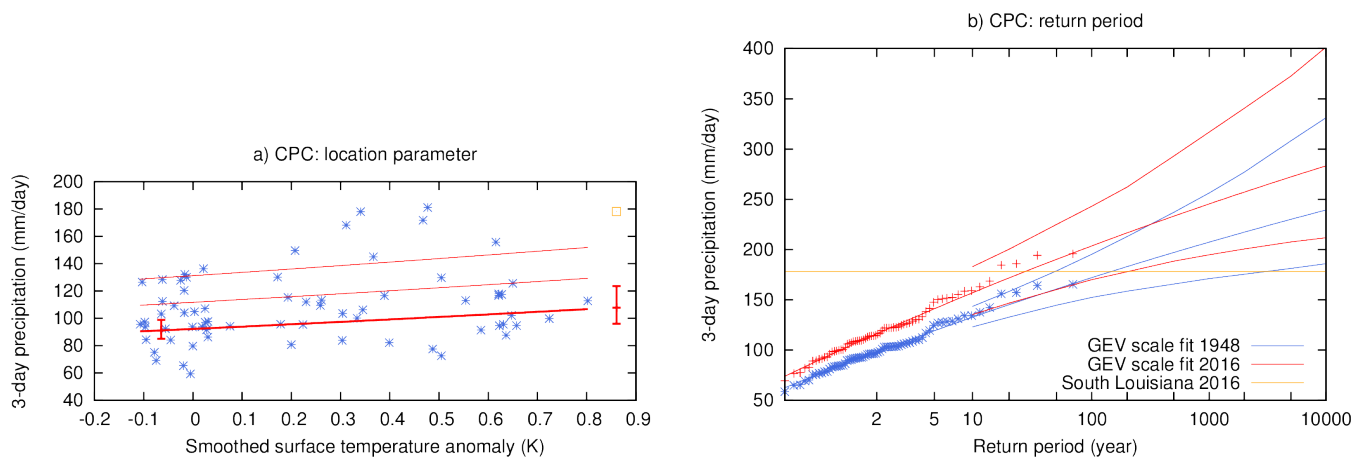
388 **Figure 4:** Fit of the spatial and annual maximum 3-day average GHCN-D station precipitation on the Central U.S. Gulf
 389 Coast to a GEV that scales with smoothed global mean surface temperature. (a) Observations (blue marks), location
 390 parameter μ (thick red line), $\mu + \sigma$ and $\mu + 2\sigma$ (thin red lines versus global mean temperature anomalies), the two vertical
 391 red lines show μ and its 95% confidence interval for the two climates in (b). (b) Gumbel plot of the GEV fit in 2016 (red
 392 line, with 95% uncertainty estimates) and 1930 (blue line), marks show data points drawn twice: scaled up with the trend to
 393 2016 and scaled down to 1900. The yellow square (line) denotes the intensity of the observed event at Livingston, LA.

394 3.2 Gridded analysis

395 To compare with the model data, we also analysed the CPC $0.25^\circ \times 0.25^\circ$ gridded precipitation analysis 1948–2016. Because
 396 the spatial extent of 3-day averaged precipitation extremes is larger than the grid boxes, we first averaged these to a $0.5^\circ \times 0.5^\circ$
 397 latitude-longitude grid. The highest value in 2016 is then 158.77 mm/day, which is the highest in the record. This is lower
 398 than at a single grid point due to the spatial averaging. A GEV fit of all 0.5° grid points (not shown) gives a return time of
 399 550 yr with an uncertainty from 300 to 2000 yr, compatible with the station analysis but with larger uncertainties. The
 400 probability has increased by a factor 3.5 (C.I. 2.0-11) since 1948, corresponding to an increase in intensity of 15% (C.I. 9%-
 401 24%).

402 Taking the spatial maximum of the original $0.25^\circ \times 0.25^\circ$ grid we find that the highest observed value in 2016 is
 403 178.2 mm/day on 12–14 August (534.7 mm in three days). The record is too short to draw robust conclusions from a fit of a
 404 GEV depending on global mean temperature except that the precipitation maxima also increase in this dataset (Figure 5). In
 405 this dataset, the return time for an event like 2016 anywhere on the Central U.S. Gulf Coast is currently between 9 and 200
 406 yr (best estimate 25 yr). This is about a factor 5 (C.I. 1.1-60) larger than it was around 1948, which equates to an increase in
 407 intensity for an event like 2016 of roughly 15% (C.I. 0.4%-30%).

408 As for station data, analyses of CPC similar to the ones above but for the season JAS show somewhat smaller
 409 trends, but with larger error margins. The estimated ranges of the JAS analyses and the all year analyses overlap.



410

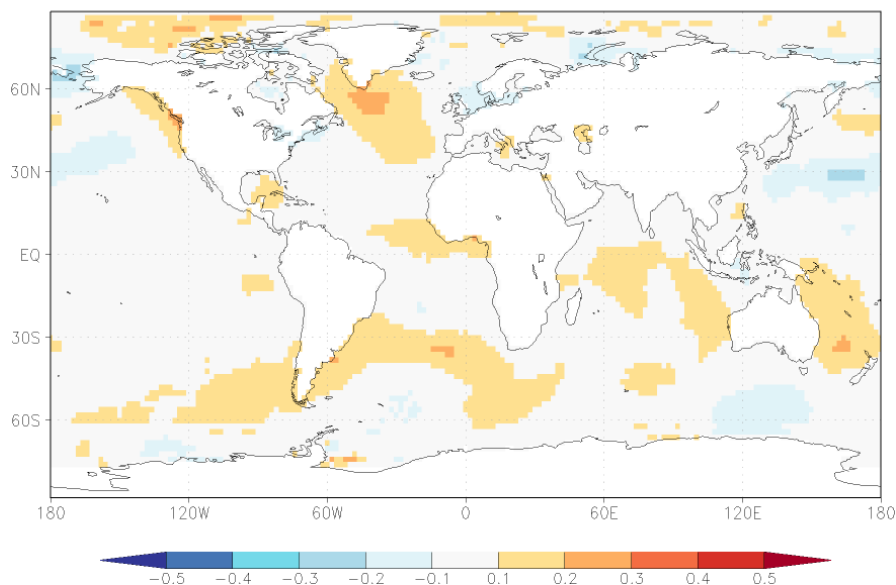
411 **Figure 5:** As Figure 4 but for the spatial and annual maximum 3-day average 1948–2016 $0.25^\circ \times 0.25^\circ$ gridded CPC analysis.

412 **3.3 Influence of natural variability**

413 We investigate the influence of natural variability on the probability of an event like south Louisiana 2016 by using indices
 414 of detrended SST as covariates in the time-dependent GEV fits. We first examine the influence of El Niño–Southern
 415 Oscillation (ENSO) by using as a covariate 6-month lagged Niño 3.4-index ($5^\circ\text{S}–5^\circ\text{N}$, $170–120^\circ\text{W}$) minus SST averaged of
 416 $30^\circ\text{S}–30^\circ\text{N}$ to remove to first order the effects of global warming. This is inspired by the heavy rain events after the
 417 1997/98 El Niño event. A comparison of recent Niño 3.4 conditions with those from a year following the strongest La Niña
 418 year (1917) in a fit of all 324 stations with more than 10 years of data suggests that anomalously warm tropical Pacific SSTs
 419 significantly ($p < 0.1$) increase the probability of an event like south Louisiana 2016, but not by much. In the year after El
 420 Niño, the probability is a factor 1.3 (C.I. 1.0–1.9) higher than in a year following a very strong La Niña. However, the
 421 maximum of stations with at least 80 years, which represents the largest events, does not show a signal, albeit with a large
 422 uncertainty of a factor 0.5 decrease to a factor 1.7 increase.

423 Simultaneous correlations with global SSTs indicate a region in the North Atlantic that has a significant relationship
 424 with Central U.S Gulf Coast extreme precipitation at $p < 0.1$ (Figure 6). Although the field significance is very low, the region
 425 is a well-known source of decadal variability and predictability (e.g., Hazeleger et al. 2013), so we still consider it a possible
 426 source of decadal variability of extreme precipitation. We use an area-average of SSTs between $45–60^\circ\text{N}$ and $50–20^\circ\text{W}$ as a
 427 covariate in the GEV fit. The region was anomalously cold in 2016, so we compare the changed probability with a warm
 428 year (2006). In this statistical analysis, North Atlantic SSTs are significantly correlated ($p < 0.01$) to Central U.S Gulf Coast
 429 precipitation (by design, as we chose the region that has a significant correlation), with recent below average SSTs
 430 decreasing the probability of an event like 2016 (risk factor 0.37, C.I. 0.11–0.81). To ascertain whether this is a physical
 431 connection and not just a coincidence by picking the region of largest correlations, we need to analyse model results.

432



433

434

435

436

Figure 6: Correlation coefficient between Central U.S. Gulf Coast spatial and annual maximum of 3-day extreme precipitation intensity and annual mean SST (ERSST v4) with a linear regression on the global mean temperature removed at each grid point.

437

4 Model evaluation

438

439

440

441

442

We here describe an evaluation of simulated precipitation extremes in the two global coupled models (model descriptions in Section 2.2). Precipitation is a notoriously difficult field to simulate, as many coupled climate models exhibit large biases (Dai 2006, Flato et al. 2013). Though FLOR-FA and HiFLOR underestimate the intensity of Central U.S. Gulf Coast precipitation extremes slightly, this bias is significantly reduced in these high-resolution models compared to standard-resolution models (Van der Wiel et al. 2016).

443

4.1 Annual cycle and intensity

444

445

446

447

448

449

450

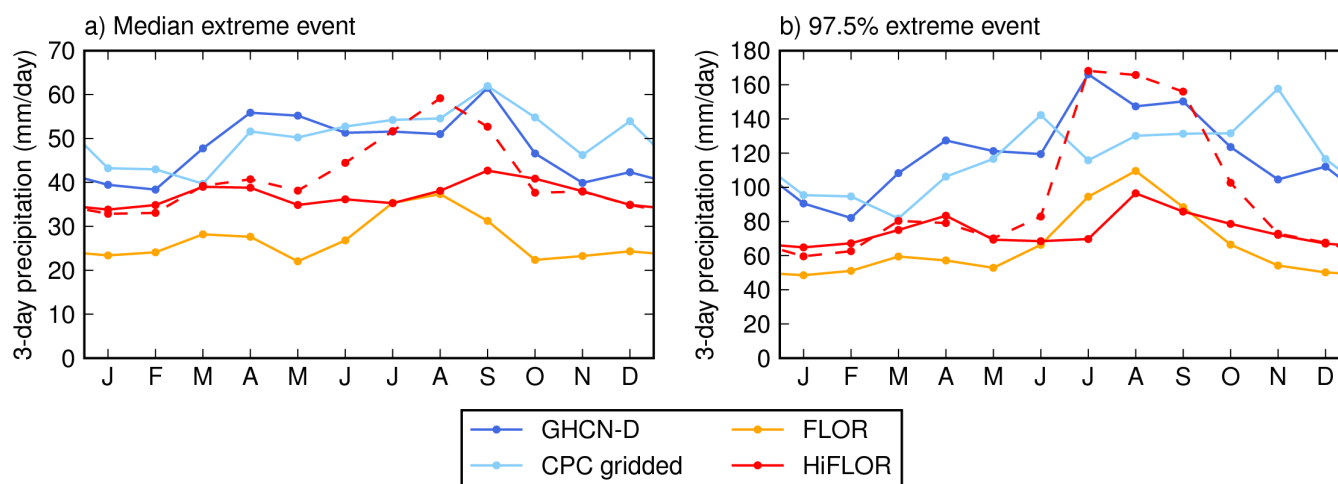
First we analyse the annual cycle of extreme precipitation intensity. We consider the median and 97.5 percentile of the monthly maximum of the spatial maximum of 3-day averaged precipitation (Figure 7). The 97.5 percentile events are of smaller magnitude than the south Louisiana observed event (100-150 mm/day versus 200 mm/day), but we consider smaller magnitude events to increase the number of events in the calculation and hence decrease uncertainties.

The observed precipitation extremes in spring and summer are generally more intense than in autumn and winter (Figure 7a). There is no agreement between the two observational products on which season sees the most intense precipitation extremes (97.5 percentile, Figure 7b), though extremes in March-October are more intense than in winter. This



451 period of stronger extremes is longer than the hurricane season, which provides a fraction of these extremes. In this region,
 452 the models underestimate the intensity of extreme precipitation, which was also noted in Van der Wiel et al. (2016). FLOR-
 453 FA has a peak season for extreme precipitation intensity in JAS which is not found in the observational data. The HiFLOR
 454 SST-restored experiment, in which global SST biases are decreased compared to the free running experiments, shows a
 455 similar peak in JAS. The HiFLOR 1990 static forcing experiment however, doesn't show this peak. Instead it has a similar
 456 annual cycle structure to the observational data, though with a smaller amplitude.

457



458

459

460

461

462

Figure 7. Annual cycle of monthly and spatial maximum 3-day averaged precipitation for point station data (GHCN-D, dark blue line), gridded observational data (CPC, light blue line) and model simulations (FLOR-FA, orange line, and HiFLOR, red lines). For HiFLOR the 1990 static forcing experiment (solid red line) and the variable forcing SST-restored experiment (dashed red line) are included. Shown are (a) the median value of the monthly extremes and (b) the 97.5 percentile.

463

4.2 Meteorological conditions

464

465

466

467

468

469

470

471

472

473

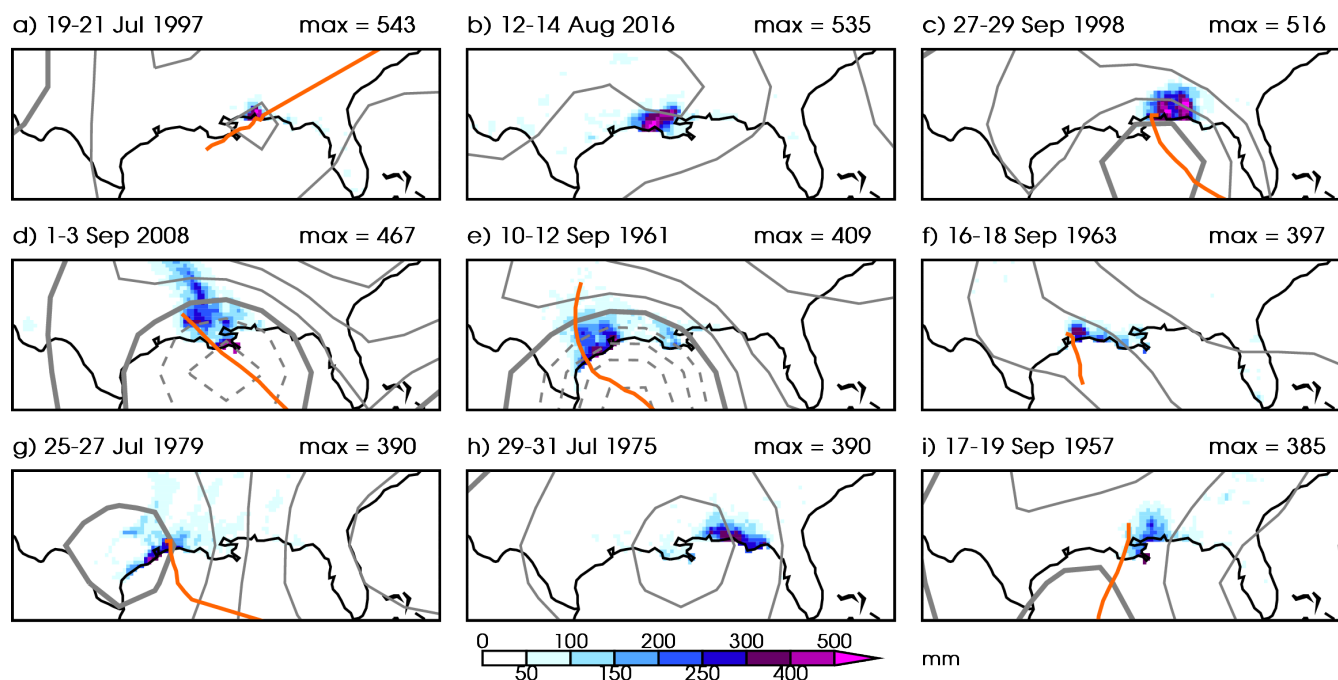
Next, we investigate the meteorological conditions generating extreme precipitation events in both models and compare these to the observed ones. For this analysis we consider the longest static forcing experiments for each model: 1860 for FLOR-FA and 1990 for HiFLOR and the CPC gridded precipitation analysis. The selection of these events is limited to the region of interest (Central U.S. Gulf Coast) and the months JAS to facilitate comparison against the south Louisiana event.

Precipitation totals and circulation patterns for the nine largest extreme precipitation events in the CPC analysis (JAS season only) are shown in Figure 8. Note that the 2016 south Louisiana event ranks as number 2- heavy precipitation related to Hurricane Danny in 1997 was stronger, though it was confined to a smaller area. Seven of these nine events were associated with a tropical cyclone/hurricane making landfall (78%, orange tracks are the International Best Track Archive for Climate Stewardship, IBTrACS, track estimate, Knapp et al. 2010), the exceptions are July 1975 and, as noted before, August 2016. Note that the GEV analysis in Section 3.2 was based on annual maxima, for which the ranked extreme events



474 are different than the ones shown in Figure 8 (these are nine of the top 14 events when all data is taken into account, ranks 1
475 and 2 are the same).

476



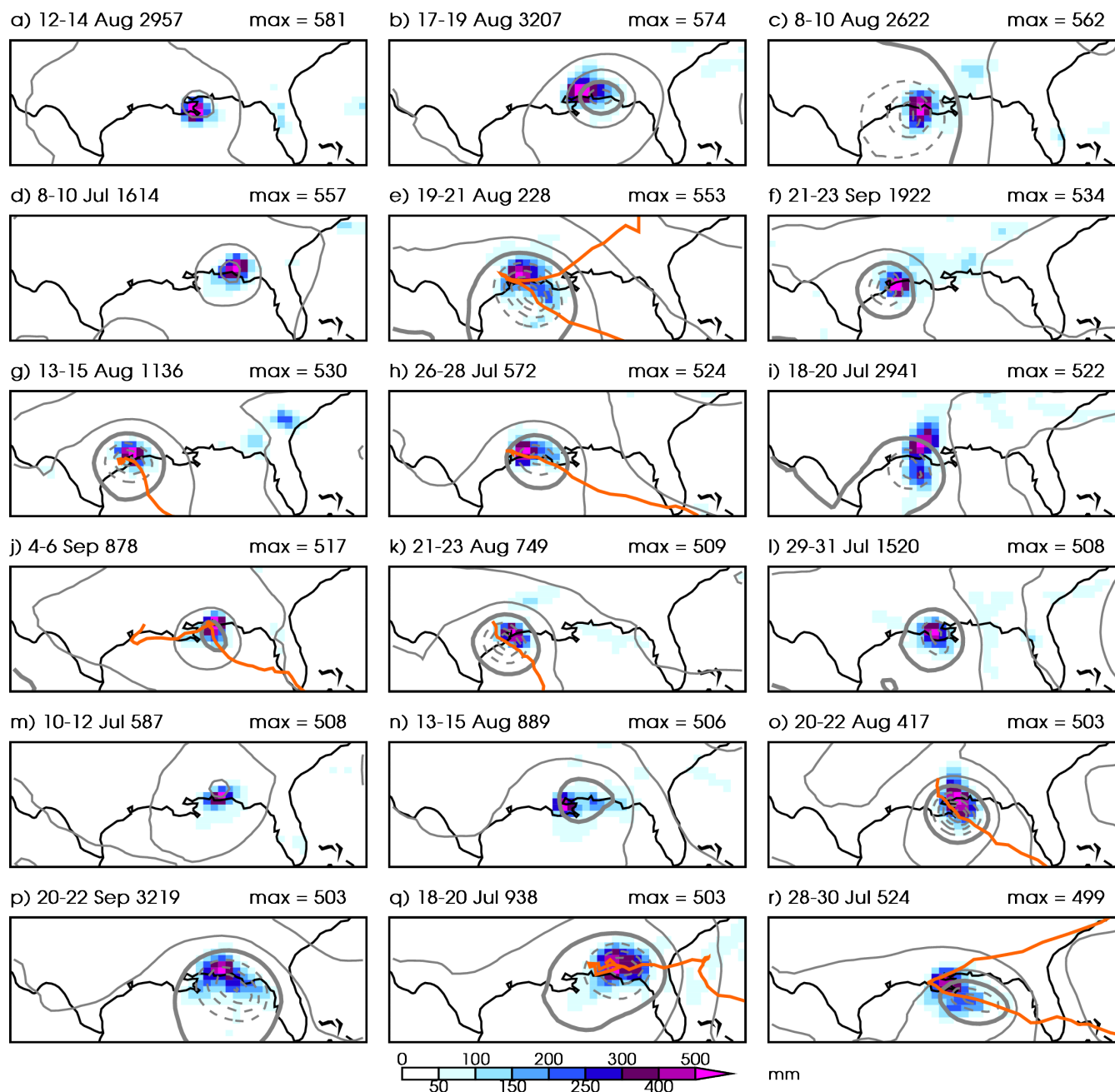
477

478 **Figure 8:** Top 9 extreme precipitation events in the Central U.S. Gulf Coast (29–31 °N, 85–95 °W) for the CPC gridded
479 precipitation analysis. 3-day precipitation sum (mm, shaded colors, as in Figure 1d), 850-hPa height for the middle day (grey
480 contours, interval 25 m, 1500 m contour thickened, lower contours dashed) from NCEP/NCAR Reanalysis 1 (Kalnay et al.
481 1996) and tropical cyclone track if system is classified as one (orange line, IBTrACS). These extreme events are calculated
482 for the three month period: JAS.

483

484

485 A similar figure for FLOR-FA is included as Figure 9. We now show the 18 most extreme events (approximate
486 return period 3530/18≈200 years) in FLOR-FA. The return period in the model for these events is much larger than the
487 return period for the observed events in the CPC analysis (approximate return period 69/9≈8 years). Despite the negative
488 bias of precipitation extreme intensity (Section 4.1), the precipitation sums for these events are therefore larger than those in
489 the observed data. All events are associated with a low pressure system, of which 8 (44%, orange tracks in Figure 9) are a
490 tropical cyclone based on the TC tracking methodology of Harris et al. (2016) as implemented in Murakami et al. (2015).
491 Note that the low pressure systems of the top 4 events do not classify as a tropical cyclone, showing the precipitation
potential of non-tropical cyclone low pressure systems in the model.



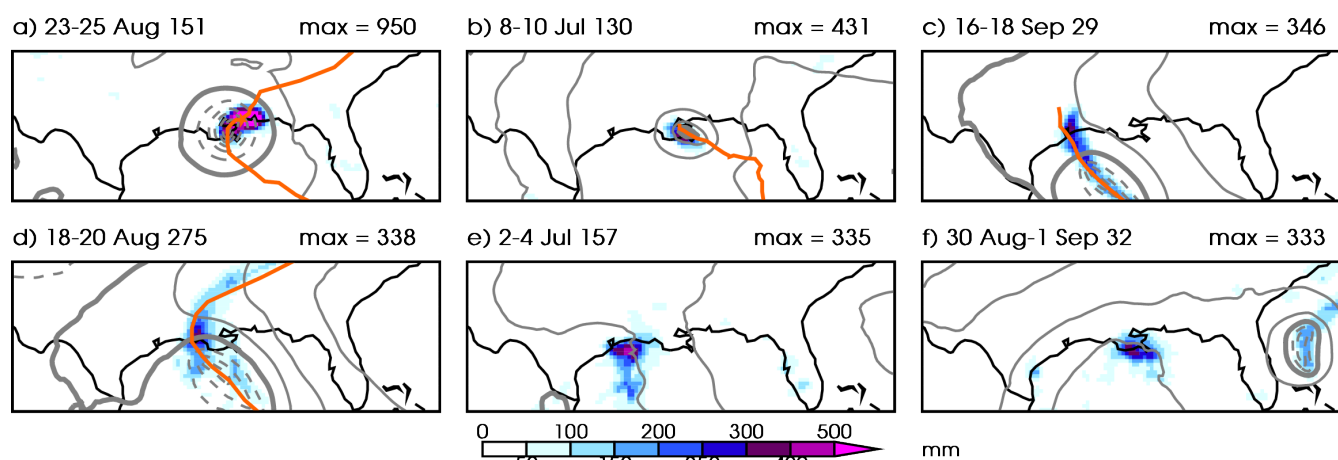
492
 493
 494
 495
 496

Figure 9: As Figure 8 but for the top 18 maximum extreme precipitation events in the 1860 FLOR-FA static forcing experiment. Note that years are model years and do not resemble dates on the real world calendar and that the model provides precipitation information over ocean grid boxes too.



497 Because the HiFLOR 1990 static forcing experiment is of smaller length, it is not possible to sample the 200-year
498 return period event as was done for FLOR-FA adequately. In Figure 10 we show the 6 most extreme events (approximate
499 return period $280/6 \approx 50$ years, the top 2 events are samples of events with return periods of about 150 years). In HiFLOR the
500 most extreme precipitation events are the result of a tropical cyclone, though storm intensity (storms in Figure 10a,b are
501 tropical storms, storms in Figure 10c,d are hurricanes at the time of landfall) is not related to resulting precipitation
502 magnitude. Note that the strongest event in HiFLOR exceeds 900 mm over a 3-day period, which is much stronger than the
503 observed values in south Louisiana.

504 In conclusion, though the precipitation extremes are of smaller magnitude in both models and the annual cycle in
505 observations is not recovered well (Section 4.1), the meteorological system leading to these precipitation extremes in JAS
506 are realistic and resemble observed systems (Section 4.2).



507 **Figure 10:** As Figure 8, but now for the top 6 maximum extreme precipitation events in the 1990 HiFLOR static forcing
508 experiment. Note that years are model years and do not resemble dates on the real world calendar and that the model
509 provides precipitation information over ocean grid boxes too.
510

511 5 Model analysis

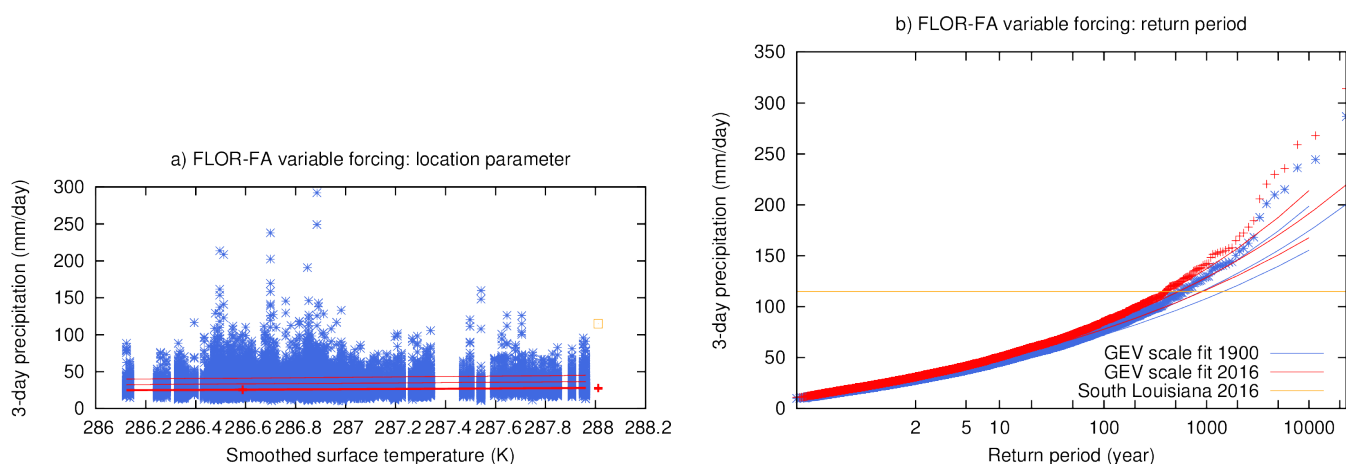
512 In order to attribute the observed trend to external forcing we use global climate models that isolate the different forcings.
513 The model and experimental description can be found in Section 2.2.

514 5.1 FLOR-FA

515 A fit of all land grid boxes ($0.5^\circ \times 0.5^\circ$, 23095 data points) to a time-dependent GEV distribution is shown in Figure 11. The
516 uncertainties take into account the dependencies by moving spatial blocks of 7.7 grid points on average. In contrast to the
517 observations (Figure 3) the distribution cannot be described with a single GEV function: the extremes with return times



518 larger than about 100 years (80 mm/day) diverge from the fit that is determined mainly by the less extreme precipitation
 519 events. This so-called 'double population' problem results from different meteorological mechanisms for extreme events. We
 520 therefore cannot use this fit for attribution.



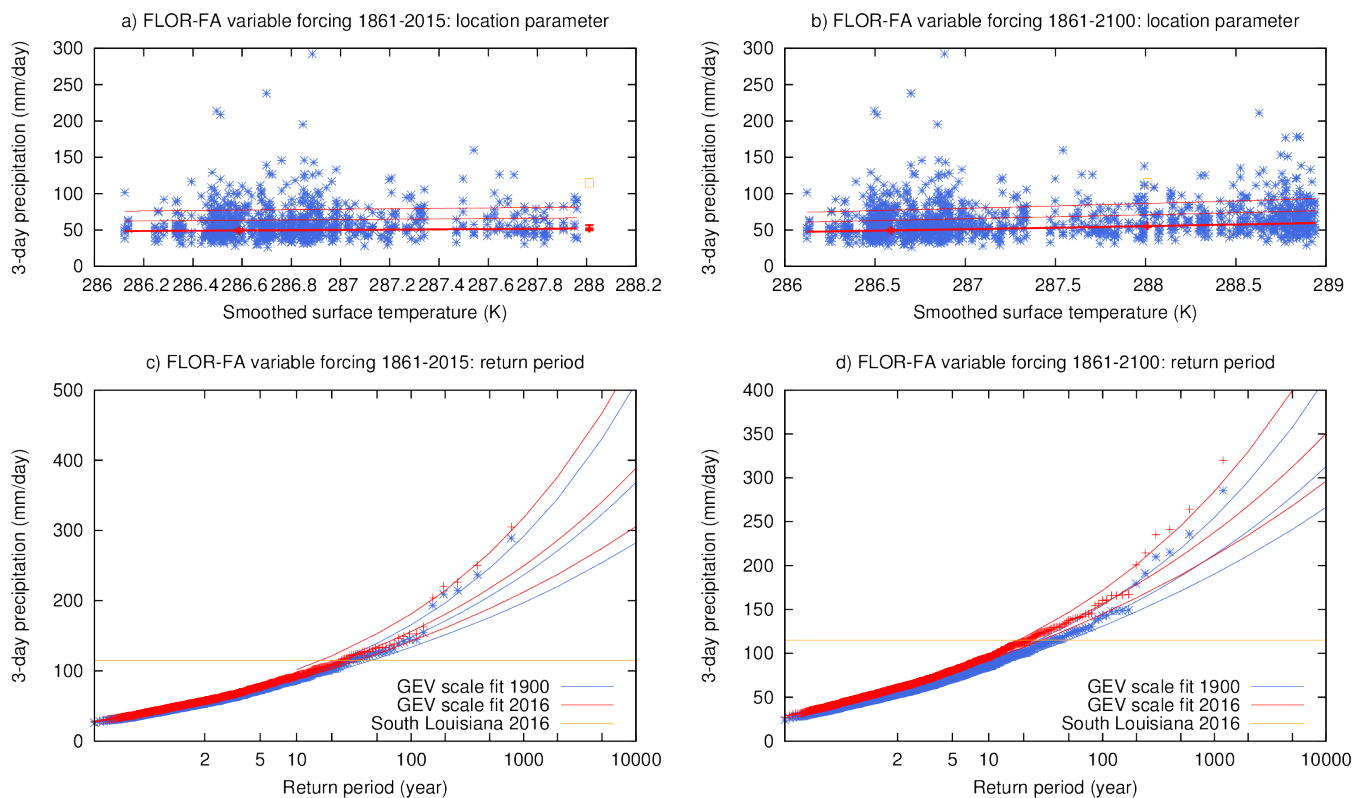
521 **Figure 11:** As Figure 4 but for the annual maximum 3-day average precipitation in the FLOR-FA variable forcing
 522 experiment (based on complete experiment, 1861-2100).
 523

524
 525 Taking the spatial maximum of all grid boxes selects only the high end of the distribution. Figure 12a,c shows the
 526 GEV fit to these extremes using data for simulated years 1861-2015. The fit is still not completely satisfactory as the highest
 527 five events (all in the early years of the experiments) fall on the upper boundary of the 95% C.I. around the fit to the rest of
 528 the distribution. Due to this, the shape parameter ξ and scale parameter σ of the GEV distribution are higher than they are in
 529 the observations. Because of model bias, we adjust the model amplitude of extremes to obtain the same return time as that in
 530 observational data, of around 30 years (115 mm/day). This gives a trend in this model that is significantly greater than zero
 531 at $p < 0.05$ (one-sided). However, the factor 1.3 (C.I. 1.0-1.9) increase in probability, corresponding to an increase in intensity
 532 of 5% (C.I. -1%-14%), is much less than the observed one.

533 Assuming that the relationship with global mean surface temperature does not change in the model world until
 534 2100, in spite of a different mix of anthropogenic forcings (greenhouse gases and aerosols), we can improve the signal-to-
 535 noise ratio of the fit by using all data in the variable forcing experiment (Figure 12b,d). For the spatial and annual maximum
 536 of 3-day averaged precipitation this gives an increase in probability of a factor 1.8 (C.I. 1.4-2.0) corresponding to an increase
 537 in intensity of 11% (C.I. 7%-12%) up to now.

538 Analogous analyses but for the season JAS show similar results, although with larger error margins. We looked for
 539 an effect of ENSO in the long static forcing experiment in the same way as in the observations. This does not show any
 540 influence of El Niño averaged over the 12 months July–June preceding the year of extreme precipitation events.

541



542

543 **Figure 12:** As Figure 4 but for the annual and spatial maximum 3-day average precipitation in the FLOR-FA variable
 544 forcing experiment. (a,c) taking into account years 1861-2015, (b,d) taking into account 1861-2100.

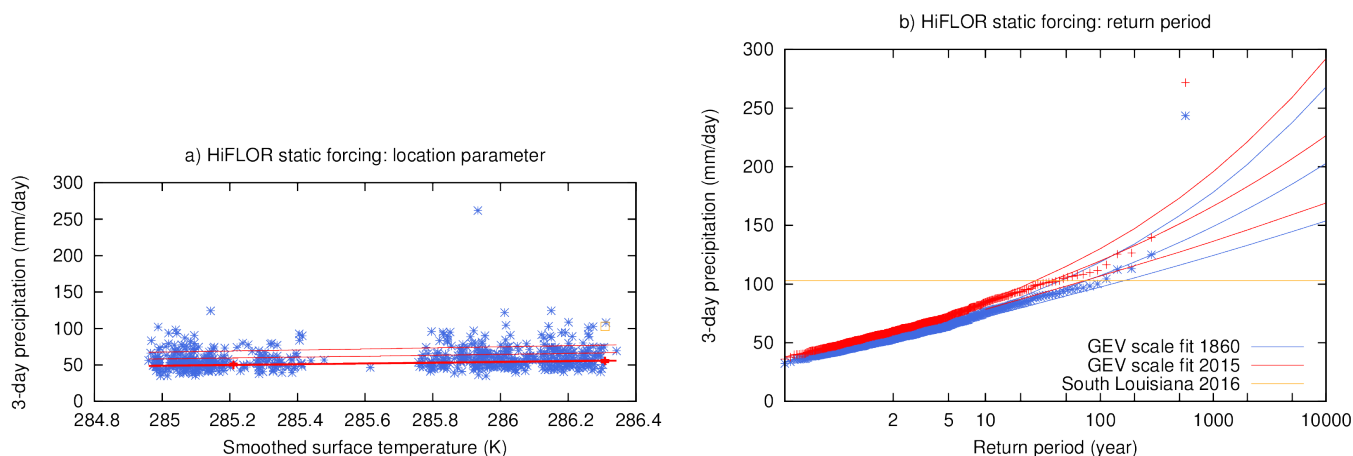
545 **5.2 HiFLOR**

546 The HiFLOR model at a higher 25 km resolution has a more realistic seasonal cycle, but underestimates extreme
 547 precipitation by 25% for a 1 in 1 year event and by 35% for 1 in 1000 year extremes. We correct for this bias by defining our
 548 event to have the same return time as the gridded observations in 2016, that is, 103 mm/day. We concatenated the four static
 549 forcing experiments that we have available, leaving out the first 20 years of each, to create a 655-year record. To decrease
 550 dependencies we averaged 2×2 grid boxes into a 0.5° grid, this results in each grid box being correlated with 10.3 others with
 551 $r > 1/e$ on average.

552 As was found for FLOR-FA, the GEV fit to all grid points results in a double population, therefore we disregard
 553 that analysis and instead focus on the spatial maximum precipitation extreme. Similar for FLOR-FA, taking the spatial
 554 maximum of this 50 km dataset selects mainly events in the more extreme population and does give a good fit to the GEV
 555 distribution (Figure 13). The outlier event is a tropical cyclone in the 1990 static forcing event, that was discussed in Section
 556 4.2 (Figure 10a). The external forcing, which is the only change between the static forcing experiments, causes an increase in



557 probability of a 103 mm or stronger event of a factor 2.0 (C.I. 1.4-2.5), in agreement with the FLOR-FA experiment up to
 558 2100 (Figure 12b,d). This corresponds to an increase in intensity of 10% (C.I. 5%-12%).



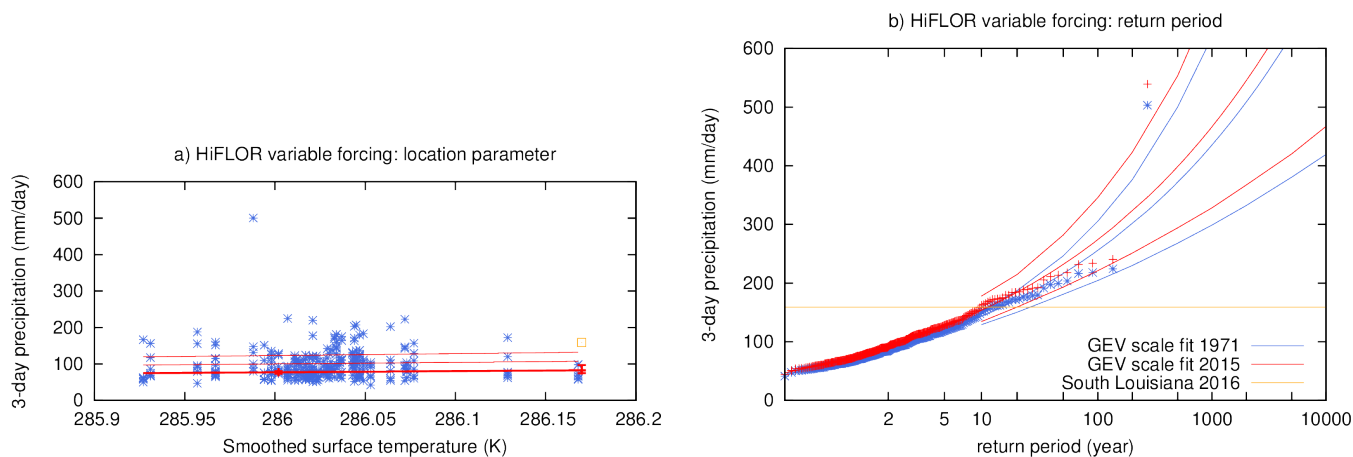
559
 560 **Figure 13:** As Figure 4 but for the annual and spatial maximum 3-day average precipitation in the HiFLOR static forcing
 561 experiments.
 562

563 An analysis of these data using the annual averaged detrended Niño3.4 index lagged by 6 months as covariate
 564 shows a relatively strong influence of El Niño in this model, with an increase in probability from the year following
 565 strongest La Niña to the strongest El Niño of a factor about 4.2 (C.I. 1.7–6.7).

566 We followed the same procedure on the six ensemble members of the variable forcing HiFLOR experiment (1971–
 567 2015). These simulations do not have a negative bias in extreme precipitation. The restored SSTs eliminate a 2 K cold bias in
 568 the subtropical Atlantic that is present in the static forcing experiments, which may have caused the bias in precipitation
 569 extremes on the U.S. Central Gulf Coast in those simulations. Again there is one outlier event with 452.8 mm/day over three
 570 days, 1351 mm total.

571 The spatial and annual maximum of 3-day averaged extreme precipitation increases by a factor 1.8 (C.I. 1.2–3.3) in
 572 these experiments over the period 1971–2015, corresponding to a change in intensity of 14% (C.I. 4%–27%), Figure 14.
 573 Although the restoring of SSTs increases the fidelity of the simulation, it also includes the non-forced natural variability of
 574 the real world, so these numbers do not isolate the forced change but show the full change including the effects of natural
 575 variability. Assuming these are small compared to the trend we can extrapolate to the full change since 1900; the period
 576 1971-2015 only includes about 2/3 of global warming since preindustrial times. This translates to a factor 2.4 (C.I. 1.3–6)
 577 increase in probability and 22% (C.I. 6%–41%) in intensity, which is very similar to the trend found in the observational
 578 data.

579 Analyses of the season JAS show similar to somewhat smaller trends, but with larger error margins, overlapping the
 580 all-year error margins.



581

582 **Figure 14:** As Figure 4 but for the annual and spatial maximum 3-day average precipitation in the HiFLOR variable forcing
583 restored SST experiments.

584 6 Summary

585 In this section we summarize the principal observational and model-based results as described in Sections 3 and 5. We have
586 analyzed two observational data products (GHCN-D point station data and CPC 0.25°×0.25° gridded analysis), to estimate
587 the probability, and changes in probability and intensity of a 3-day precipitation event as large as that observed in south
588 Louisiana 2015. The analysis was confined to the Central U.S. Gulf Coast (29–31 °N, 85–95 °W) and relies on time-
589 dependent GEV fits to the data. First we investigated probabilities and changes at a single station, i.e. the probability of such
590 an event *at a fixed place* in the region. Second we investigated regional probabilities and changes, i.e. the probability of such
591 an event *anywhere* in the region. The spatial scale of the most extreme precipitation events is significantly smaller than the
592 region considered, therefore the second probability is lower than the first. To attribute the observed changes to forced
593 anthropogenic climate change, we repeat the analysis using high-resolution global climate model data from GFDL FLOR-FA
594 and GFDL HiFLOR. GEV fits for the local analysis were unsatisfactory, therefore we only report the regional change in
595 probabilities.

596 The expected return period of a comparable 3-day precipitation event at a single station as high as the maximum
597 observed is 450 to 1450 year, best estimate 550 year. Return periods like these are often written as a "1 in 1000 year event".
598 The return time for observing an event anywhere in the region is lower: between 11 and 110 year. All observational analyses
599 found clear positive trends, with an increase in probability for the regional event of about a factor 6.3 (97.5% certain more
600 than 2.1), and an increase in intensity of 12% to 35% (Table 3). Estimates based on CPC gridded data are comparable but
601 have larger ranges due to the shorter period of data availability.



602 **Table 3:** Summary of observed (first two rows) and modeled (third row and down) changes in regional rainfall extremes in
 603 Central U.S. Gulf Coast.

Data source (years used for calibration)	Baseline regional return period for 2016 event (95% confidence range, observations only)	Years change calculated over	Change of return period in present day over given years (95% confidence range)	Change in intensity of regional 30-year return event in 2016 since beginning of record (95% confidence range)
GHCN-D rain gauges, minimum 80 year data (1930-2016)	30 year (11 - 110)	1930-2016	6.3× (2.1 ... 50)	+25% (12% ... 35%)
CPC 0.25°×0.25° gridded data (1948-2016)	25 year (9 - 200)	1948-2016	5.4× (1.1 ... 60)	+15% (0.4% ... 30%)
FLOR-FA variable forcing experiment (1861-2015)		1900-2016	1.3× (1.0 ... 1.9)	+5% (-0.5 ... 14%)
FLOR-FA variable forcing experiment (1861-2100)		1900-2016	1.8× (1.4 ... 2.0)	+11% (7% ... 12%)
HiFLOR static forcing experiment (1860, 1940, 1990, 2015)		1860-2015	2.0× (1.4 ... 2.5)	+10% (5% ... 12%)
HiFLOR variable forcing experiment (1971-2015), extrapolated to 1900-2015		1900-2015	2.4× (1.3 ... 8)	+22% (6% ... 41%)

604

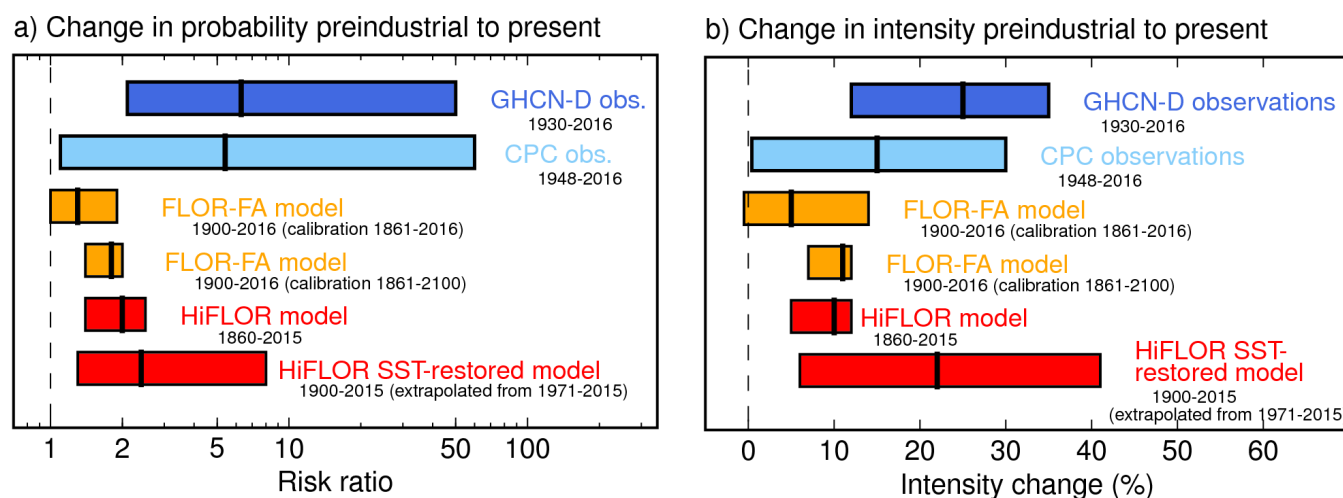
605 The sensitivity of precipitation extremes from both models is consistent with that estimated from the gridded
 606 observations. The lower-resolution FLOR-FA model shows lower trends than the HiFLOR model. For the HiFLOR model
 607 the sensitivity estimated from the SST-restored experiment for 1971–2015 is larger than that from the coupled simulations.
 608 Taking into account all modeling results, the probability of an event like south Louisiana 2015 has increased at least by a
 609 factor 1.4 due to radiative forcing; the two HiFLOR experiments and the analysis of the full dataset from FLOR-FA suggest
 610 central values close to a doubling of probability. Such an increase may be translated to what was once a 1/100 year event
 611 somewhere in the Central U.S. Gulf Coast, should now be expected to occur on average, at least once every 70 years, likely
 612 even more common. This trend is expected to continue over the 21st century as past and projected future greenhouse forcing
 613 continues to warm the planet.

614 The evidence for an influence of the strong 2015/2016 El Niño increasing the probability of the 2016 event is
 615 equivocal. The full station dataset shows a statistically significant but small increase in probability, but we do not find the
 616 same for the spatial maximum, which represents the strongest events. The FLOR-FA model similarly does not have an
 617 ENSO effect, whereas the HiFLOR model again shows a higher probability after a large El Niño. We have found some



618 evidence for decadal Atlantic variability affecting precipitation in the observations, which would have decreased the
 619 likelihood in 2016 if confirmed.

620



621

622 **Figure 15:** Summary of observed (GHCN-D, CPC, blue colors) and modeled (FLOR-FA, HiFLOR, yellow, red color)
 623 changes in regional precipitation extremes in Central U.S. Gulf Coast. Ranges written in black are the time periods for which
 624 the change is shown over. Calibration for the calculations is done over separate time periods for noted models. See Table 3
 625 for specific numeric values.

626 7 Discussion

627 We have presented a rapid attribution to climate change and climate variability of the south Louisiana intense precipitation
 628 event. Here we lay out the crucial assumptions made to conduct our assessment, further lines of inquiry to investigate the
 629 validity of the crucial assumptions and the sensitivity of our results to changes in these assumptions, suggestions for further
 630 study on related topics not investigated here, and questions that arise from this work. Finally, we note some societal impacts
 631 and management implications of the findings.

632 7.1 Crucial assumptions

633 In performing these analyses, we have made the following crucial assumptions about the observations, models, the statistical
 634 distribution of precipitation extremes, and the relationship between temperature and precipitation extremes. We have tested
 635 the sensitivity of our results to some of these assumptions in the results sections (Sections 3-5) and discuss them below.

- 636 1) We assume that the local, annual maxima of 3-day averaged precipitation over the region of analysis (29–31 °N,
 637 85–95 °W) can be grouped together, and that their statistical distribution follows a GEV distribution. Underlying
 638 this assumption is that the region has homogeneous extreme precipitation characteristics (Figure 1f). Furthermore,



639 we assume that all the annual maxima of 3-day averaged precipitation are drawn from the same statistical
640 distribution, in spite of the many different mechanisms that lead to extreme precipitation in this region, and that this
641 distribution can be represented well by a GEV distribution. We further assume that the spatial maximum over the
642 region can also be described by a GEV.

643 2) We assume that analyzing all seasons together provides a fuller distribution of the population of extreme
644 precipitation events than isolating the analysis to seasons proximate to August (the month in which the south
645 Louisiana event occurred). In part, the choice to analyse annual extreme events was motivated by the fact that a
646 variety of meteorological phenomena can lead to extreme precipitation in this region, flooding can occur in any
647 season, and precipitation extremes may change in various seasons (Lehmann et al. 2015, Van der Wiel et al. 2016).
648 All extreme value analyses were repeated focusing only on the JAS season and the qualitative nature of the results
649 was the same as those presented.

650 3) We assume that the inhomogeneities in point station data due to station changes, incomplete records and geographic
651 coverage are smaller than the trends and have no coherent sign. We have checked this by performing the analysis on
652 all stations and for a subset of stations with long (at least 80 year) records and sufficient (0.5°) spatial separation.

653 4) We assume that the methods that create the gridded observationally-based precipitation data result in an accurate
654 representation of 3-day average precipitation at the grid scale. The decorrelation scale of 3-day precipitation is
655 about twice the grid scale, so the largest uncertainty is the inhomogeneous distribution of the gauge stations in space
656 and time. A comparison of the results with point station data shows that the differences are not large.

657 5) We assume that, for the assessment of trends in GEV statistics, global mean surface temperature represents a
658 relevant covariate to capture the *a priori* expected connection between precipitation extremes and temperature (e.g.,
659 O’Gorman 2015). A physical motivation for this expected connection is the dependence of the saturation specific
660 humidity of air on temperature through Clausius-Clapeyron (see Section 1). The underlying assumption is that
661 multi-decadal temperature changes exhibit “pattern scaling”, such that global mean temperature change is a
662 sufficient parameter to describe the long-term changes of temperature; furthermore, global-mean temperature helps
663 increase the signal-to-noise ratio of fits to temperature changes. If there is substantial spatial heterogeneity to
664 temperature changes on multi-decadal timescales, the assumption that global mean temperature is the relevant
665 metric becomes suboptimal. Furthermore, if dynamical changes (e.g., changes in the statistics of storms, changes in
666 the dominant moisture sources for extremes, etc.) dominate the observed multi-decadal precipitation extreme
667 changes, this assumption will also be suboptimal.

668 6) We assume that the probability density function of precipitation extremes scales with a covariate, for example
669 (smoothed) global mean temperature and does not exhibit other changes in shape. This assumption is supported by
670 large-sample statistics from modelling experiments such as Weather@Home (Massey et al. 2015) in other regions,
671 but it is not *a priori* obvious that these results should also hold for the Central U.S. Gulf Coast with its wide variety



672 of weather phenomena causing extreme precipitation. Furthermore, the Massey et al. (2015) results were from
673 models of resolution too low to resolve many of the meteorological phenomena that lead to extreme precipitation
674 (e.g. tropical cyclones) in this region.

675 7) We assume that, beyond an initial rapid (~20 year) adjustment to different static radiative forcings, the statistics of
676 precipitation extremes in the static forcing model experiments depend on global mean temperature in the same way
677 as the changes arising from slow drift due to top of the atmosphere radiative disequilibria and slow ocean
678 adjustment. The latter changes are smaller than the forced trend, so the impact of slow model drift on the results is
679 small.

680 8) We assume that the CMIP5 historical forcings (1860-2005) and RCP4.5 forcings (2005-2100), as implemented in
681 the models, are sufficiently accurate representations of the actual changes in radiative forcing that occurred in the
682 real climate system to allow meaningful comparison of modeled changes in precipitation extremes to those
683 observed.

684 9) We assume that the FLOR-FA and HiFLOR modeled responses to changes in radiative forcing are meaningful
685 estimates of the sensitivity of precipitation extremes in the real climate system, since these models capture multiple
686 physical factors affecting precipitation extremes in a physically-based and internally-consistent framework. This
687 assumption is motivated in part because of the ability of these models to simulate large-scale precipitation and
688 temperature over land (e.g., Van der Wiel et al. 2016; Delworth et al. 2015; Jia et al. 2015, 2016), precipitation
689 extremes over the U.S. (Van der Wiel et al. 2016), modes of climate variability (e.g., Vecchi et al. 2014; Murakami
690 et al. 2015); the meteorological phenomena that lead to precipitation extremes and their relationship to modes of
691 climate variability (e.g., Vecchi et al. 2014; Krishnamurthy et al. 2015; Murakami et al. 2015, 2016; Zhang et al.
692 2015, 2016; Pascale et al. 2016); and that these models show skill at seasonal predictions of large-scale climate,
693 regional hydrometeorology and the statistics of weather extremes across a broad range of climatic regimes (e.g.,
694 Vecchi et al. 2014; Jia et al. 2015, 2016; Yang et al. 2015; Msadek et al. 2015; Murakami et al. 2015, 2016).
695 However, it is important to note that climate models can show a range of global and regional climate sensitivities to
696 changing radiative forcing (e.g., Kirtman et al. 2013, Collins et al. 2013)

697
698 These assumptions were crucial to enable a rapid assessment of the climate context of the extreme precipitation of
699 the August 2016 south Louisiana event. Subsequent analyses should further assess the validity of these assumptions, and the
700 quantitative impact of failures in their validity. Below we outline our present evaluation of the implications of these choices
701 and potential areas of further research.

702 Sensitivity experiments should be produced by varying the parameters of our study. We did not conduct analysis of
703 how the size of our defined box for the Central U.S. Gulf Coast affects our results (crucial assumption 1). If the region is
704 altered to remove points that have greater risks relative to those included, the findings may change. Changes in extreme



705 precipitation risks in the Central U.S. Gulf Coast should not be applied elsewhere without further investigation. Temporally,
706 we were able to validate the seasonal distribution of precipitation extremes in models and observations (Section 4.1), and
707 redid the analysis for JAS only, which gave larger uncertainties and somewhat smaller trends (crucial assumption 2). Future
708 work could further quantify seasonal differences in extremes and their response to climate forcing. Similarly, to sample the
709 spread in sensitivity to future RCP forcings (crucial assumption 8, used for any modeled years beyond 2005), our results may
710 be revised with different climate forcings. For the near term however, this is likely not an issue in HiFLOR (used to produce
711 climates for 2005-2015 in the static forcing and nudged SST runs) as climate variability tends to be greater than the climate
712 response to different scenarios during this time period (Forster et al. 2013; Hawkins and Sutton 2009; Kirtman and Power
713 2013), but may affect future climate results in the FLOR-FA variable forcing experiment at the end of the century (2100,
714 Hawkins and Sutton 2009). Finally, the appropriateness of GEV fits in general should be tested (crucial assumptions 1,6).

715 Sensitivity experiments of our results to model bias and integration length (or length of the observed record) should
716 be produced (crucial assumptions 3 and 7). Short records limit the reliability of the statistics of precipitation extremes. This
717 is important for our model validation of the annual cycle of extremes (Section 4.1) and for the comparison of modeled and
718 observed GEV fits (Section 5). The statistics of precipitation extremes in HiFLOR are closer to those observed than the
719 statistics in FLOR-FA. However, we note that the model experiments with FLOR-FA are significantly longer and therefore
720 provide better statistics of its (biased) climate than the experiments with HiFLOR or the observed record. It cannot thus be
721 fully-excluded that the double distribution of extremes in FLOR-FA or the large peak in JAS in extreme precipitation
722 intensity is purely a result of model bias.

723 A portion of the beginning of the static forcing experiments have been disregarded to allow the model to spin-up in
724 response to radiative forcing. GEV fits were originally calculated by disregarding the first 10 years of data to allow for spin-
725 up, but was extended to 20 years to provide the simulated climate more time to approach equilibrium (crucial assumption 7).
726 The results are only altered slightly by this sensitivity test. Given the length of the available ensemble suite of static forcing
727 experiments, disregarding more years in the beginning of the simulation would reduce our ability to sample extremes. With
728 longer integrations of static forcing experiments and additional ensemble members, we would have more information to
729 assess how model spin-up may affect our results. Similarly, longer integrations would allow for an assessment of the impact
730 of model drift due to ocean adjustment (crucial assumption 7).

731 The attribution to climate change presented here depends on our assumption that changes in precipitation extremes
732 scale with global mean temperature and do not arise from changes in the shape of their underlying distribution (crucial
733 assumptions 5 and 6). The thermodynamic basis of this assumption is based on a large body of research (O’Gorman 2015),
734 however as noted before there is a large variety of synoptic systems that may cause precipitation extremes in the Gulf Coast
735 region. It is not obvious that possible impacts of changes in synoptic weather patterns scale with global mean temperatures.
736 For example, the frequency, track location and/or intensity of tropical cyclones (responsible for 7 out of the 9 most extreme
737 events in JAS were related to tropical cyclones, Figure 8) can each change in complex ways that need not scale with each



738 other or global mean temperature (e.g., Vecchi and Soden 2007; Murakami and Wang 2010; Emanuel and Sobel 2013;
739 Emanuel et al. 2013; Knutson et al. 2013; Vecchi et al. 2013; Walsh et al. 2015), and could cause changes to the statistics of
740 extreme rainfall in the Central U.S. Gulf Coast. Further research must investigate what the impact of dynamic changes (e.g.
741 frequency of occurrence of various synoptic systems, dominant moisture sources, precipitation efficiency) is on the
742 presented trend of precipitation extremes.

743 To investigate the sensitivity of the results to the chosen observational data sets (both based on rain gauge
744 measurements, crucial assumption 3 and 4), we suggest repeating the current analysis with an independent observational
745 estimate of current and historical precipitation along the Gulf coast (e.g. estimates based on satellite data). Furthermore,
746 though we use two global climate models (FLOR-FA and HiFLOR, crucial assumptions 7 and 9) and various experimental
747 setups (static radiative forcing, time-varying radiative forcing and restoring observed SST variability), the models are part of
748 the same NOAA/GFDL family. Consequently, they exhibit similar patterns of (surface temperature) bias and rely on the
749 same parameterization schemes for precipitation. Further inquiry for understanding model-specific biases that may impact
750 the results may still be warranted. For example, there is a North Atlantic cold bias in the models, thought to be connected in
751 part to inadequate eddy parameterizations and a resulting cloud feedback (Delworth et al. 2006; Delworth et al. 2012; Vecchi
752 et al. 2014; Murakami et al. 2015). This may be the source of higher magnitudes of modeled extreme precipitation found due
753 to climate variability in the HiFLOR restored-SST experiments. An assessment using different climate models would
754 therefore add value to allow for a sampling of risk across models, in addition to across experimental setups. These will be
755 available shortly in the HighResMIP project (Haarsma et al 2016).

756 **7.2 Future work and broader impacts**

757 As described in the introduction and methods, we have purposefully focused our present assessment on one aspect
758 of the flooding problem: the risk of extreme precipitation events that have the potential to produce inland flooding. We have
759 provided provisional streamgauge data in the introduction (Figure 2) to illustrate the effect of the August 2016 event, but
760 have not examined flood risks in the region from streamgauge data directly. Part of the reason for this is that real-time
761 streamgauge data is provisional and subject to revision, which can be exacerbated during a flood when gauges can be
762 overtopped and have missing data due to high water volumes or streamgauge malfunctions (Rantz 1982). The USGS advises
763 users to cautiously consider the use of provisional streamgauge data for decision making (official USGS provisional policy
764 available: <https://water.usgs.gov/wateralert/provisional/>). A complimentary modeling study of land surface conditions and
765 interactions with the river environment also requires a more local modeling approach, potentially with a hydrologic model
766 with information on the river system and small scale water processes, and conceivably including an estimate of the impact of
767 direct human impacts (through urbanization, water diversion and management, etc.) which under our time constraints, data
768 access, and present capabilities of our climate models was not feasible.



769 It is important to distinguish extreme precipitation events that are the topic of this study, motivated by the August
770 2016 rain event that led to devastating “freshwater” or “inland” flooding in south Louisiana, from events that lead to
771 “coastal” or “saltwater” flooding. In particular, the climate change context of saltwater flooding must include an assessment
772 of the regional sea level change contributions and meteorological conditions that can influence these types of events (e.g.,
773 Katsman et al, 2008, Sterl et al, 2012, Lin et al. 2012, 2014, Little et al. 2014). While certain meteorological conditions, such
774 as landfalling tropical cyclones, can lead to both freshwater and saltwater flooding (e.g., Lin et al. 2012, Villarini et al.
775 2014), the assessments and discussions presented here are only relevant to extreme rainfall events that have the potential to
776 initiate inland flooding; we do not address changes in storm surges, nuisance flooding (Moftakhari et al. 2015) or other
777 saltwater flooding events.

778 Dependence of the statistics of extreme precipitation events in the Central U.S. Gulf Coast on large-scale climate
779 drivers could provide a scientific basis for seasonal predictions of the odds of these events, much as is now regularly done
780 for the statistics of hurricanes. However, as we show in Section 3.3, we are unable to find strong connections between the
781 statistics of these extreme precipitation events and modes of SST variability (e.g., ENSO), which suggests the possibility for
782 limited seasonal predictability for these events beyond the multi-decadal increase in probability from long-term climate
783 warming. However, potential sources of predictability may be uncovered by future refined analyses.

784 The extent to which the changing risk of extreme rainfall events like that in south Louisiana has implications for
785 stakeholders, such as homeowners, local and federal governments, the humanitarian system, and the insurance industry, will
786 depend on details of the exposure, vulnerability and the disaster preparedness and response strategies available to each.
787 Changes to the physical system are a key factor in adaptation and decisions, but these factors operate in a complex
788 landscape. Through a disaster management lens, the increased frequency of this type of event found in this study may place
789 strains on humanitarian responders and institutions, especially in the future if this type of extreme event continues to become
790 more frequent. Knowing the change in return periods of the most extreme events can help to provide insight into how
791 humanitarian institutions can evolve to be prepared for the future; in addition to adapting to a broader trend of increasing
792 hydro-meteorological disasters globally (CRED 2015). A worthwhile topic to explore in further assessment of this and
793 related events is the extent to which public and media perception both before (local preparedness, willingness to evacuate)
794 and after (nationwide media coverage and awareness of impacts) may have been impacted by the fact that the storm was not
795 named. However, there is an insufficiency of peer-reviewed literature on this topic, even as media outlets in the UK and U.S.
796 have started naming winter storms following the German example (Cutlip 2013, Van Oldenborgh et al. 2015).

797 It is essential to note that this analysis has pursued an assessment of the climate context of extreme precipitation
798 events (a “climate attribution” study) in which we evaluate the impact of climate conditions and changes in radiative forcing
799 on the probability of extreme rainfall events in south Louisiana and the Central U.S. Gulf Coast. This analysis is
800 fundamentally different in nature from (and complementary to) assessments of the synoptic chain of events that led to the
801 particular Louisiana extreme precipitation event in August 2016 (we would label that “synoptic attribution”). Synoptic



802 attribution of the event generally involves a clear chain of events that led to the extreme rainfall event in a relatively
803 deterministic fashion. Meanwhile, the climate attribution presented here is fundamentally probabilistic. Although we
804 recognize that the synoptic context of this particular extreme event is unique (in fact all events are unique in detail), we have
805 sought to understand the climate context of the probabilities of a class of events that causes extreme precipitation in the
806 Central U.S. Gulf Coast of which this event (flood-inducing extreme precipitation in south Louisiana) is a member (Otto et
807 al, 2016). Furthermore, it is possible to assess the climatic context in more detail, by assessing more proximate climate
808 drivers than global-mean temperature or radiative forcing (e.g., by looking at the impact of particular patterns of SST), or by
809 a more refined assessment of the detailed impact of the superposition of modes of climate variability and multi-decadal
810 climate change (e.g., Delworth et al. 2015, Jia et al. 2016). For any particular event a spectrum of attribution studies (from
811 purely synoptic to purely climate) could, and perhaps should, be pursued in order to unravel the various factors relevant to
812 that event. Moreover, some of these studies are feasible at rapid attribution timescales while others require more time and
813 focused resources to produce the specific and targeted modeling experiments and observational analyses.

814 Our ability to perform the climate attribution of this event was made possible by pre-existing multi-centennial
815 global simulations with high spatial resolution models, which allowed us to efficiently assess the impact of radiative forcing
816 changes on regional extreme precipitation events. These simulations, obviously, necessitated the long-term research aimed at
817 developing these high-resolution models (e.g., Putnam and Lin 2007, Delworth et al. 2012, Vecchi et al. 2014, Murakami et
818 al. 2015). Furthermore, this work was enabled a body of work using these models that provided the necessary understanding
819 of the characteristics and fidelity of these models to simulate large-scale and regional climate, and weather events over a
820 broad range of scales and phenomena (e.g., Vecchi et al. 2014; Msadek et al. 2014; Delworth et al. 2015; Jia et al. 2015,
821 2016; Murakami et al. 2015, 2016; Krishnamurthy et al. 2015; Zhang et al. 2015, 2016; Pascale et al. 2016; Van der Wiel et
822 al. 2016).

823 In particular, this paper follows on a recent analysis of the climatology and CO₂ sensitivity of extreme precipitation
824 events over the U.S. in these same models, showing that FLOR and HiFLOR in particular are uniquely capable of capturing
825 Central U.S. Gulf Coast precipitation extremes, which has large biases in coarser resolution models (Van der Wiel et al.
826 2016). Though the analysis of extreme precipitation events in Van der Wiel et al. (2016) is of a different nature (focusing on
827 much lower return period events, using different statistical methods, and focusing at the grid point scale rather than regional
828 events), the results presented there are consistent with the current analysis. The previous paper showed that in response to
829 increasing CO₂ levels in the atmosphere, precipitation extremes along the Central U.S. Gulf Coast increase in intensity, with
830 less likely events exhibiting larger fractional intensity increases.

831 We have here sought to provide a scientifically rigorous rapid assessment of the climate context of this precipitation
832 event, which had tragic consequences, to provide meaningful grounding to the public discussions of this event, given both
833 the intense interest in this specific event and our ongoing work on the general subject of climate and extremes (and
834 precipitation extremes in the U.S. in particular, van der Wiel et al. 2016). We hope that this study, including our explicit



835 discussion of the assumptions needed to pursue this accelerated assessment, will help push the scientific conversation
836 forward to improve our understanding of the risks and return periods of extreme precipitation in the Central U.S. Gulf Coast.
837 The field of rapid attribution analysis is still nascent and may one day lead to such assessments being the normal course of
838 action in response to an extreme event to help provide scientific basis for real-time discussions, and in longer-term disaster
839 response and rebuilding. Until that time, studies such as this will likely only be done for select regions and event types where
840 there is sufficient easily accessible data, and a team of scientists with the necessary expertise and ability to make time in their
841 schedules to provide a rapid assessment. We expect that these early efforts at event attribution will expand our knowledge
842 and capabilities on this subject, and facilitate further inquiry.

843 **Acknowledgements**

844 We thank Geert Lenderink, Sarah Kew, Nathaniel Johnson, Kieran Bhatia and Fanrong Zeng for their helpful comments on
845 an earlier version of the manuscript. Funding for this work was supplied by the National Oceanic and Atmospheric
846 Administration, U.S. Department of Commerce to the Geophysical Fluid Dynamics Laboratory, to the Cooperative Institute
847 for Climate Science (award NA14OAR4320106). The statements, findings, conclusions, and recommendations are those of
848 the authors and do not necessarily reflect the views of the National Oceanic and Atmospheric Administration, or the U.S.
849 Department of Commerce, or other affiliated institutions. This project was made possible through generous support from
850 donors to Climate Central's World Weather Attribution initiative and the EU project EUCLEIA under Grant Agreement
851 607085. CPC U.S. Unified Precipitation data provided by the NOAA/OAR/ESRL PSD, Boulder, Colorado, U.S. and can be
852 downloaded from: from <http://www.esrl.noaa.gov/psd/>. USGS data was obtained from the automated website and are
853 provisional and subject to revision. The data are released on the condition that neither the USGS nor the United States
854 Government may be held liable for any damages resulting from its use.

855 **Data availability**

856 NOAA GFDL climate model data is not readily available globally at all grid points and for all simulations owing to the size
857 of daily global climate model output for high resolution models with thousands of years of simulations (on the order of 100x
858 terabytes). We have made the precipitation data for the Central U.S. Gulf Coast, global temperature and ENSO data that
859 were used in this study available at the Climate Explorer: http://climexp.knmi.nl/selectfield_att.cgi.

860 **References**

861 Allen, R. and Burgess, R.: LSU AgCenter predicts floods cost state at least \$110 million in crop loss. The Advocate, viewed
862 26 August 2016. http://www.theadvocate.com/louisiana_flood_2016/article_a7689806-6946-11e6-a681-ab59c458f55c.html?sr_source=lift_amplify



- 864 American Red Cross: Louisiana Flooding: Red Cross Shelters 10,000+ After Worst Disaster Since Superstorm Sandy.
 865 *American Red Cross*, viewed August 23 2016, [http://www.redcross.org/news/press-release/Louisiana-Flooding-Red-Cross-](http://www.redcross.org/news/press-release/Louisiana-Flooding-Red-Cross-Shelters-10000-After-Worst-Disaster-Since-Superstorm-Sandy)
 866 [Shelters-10000-After-Worst-Disaster-Since-Superstorm-Sandy](http://www.redcross.org/news/press-release/Louisiana-Flooding-Red-Cross-Shelters-10000-After-Worst-Disaster-Since-Superstorm-Sandy)
- 867 American Red Cross: Needs of People in Louisiana Remain Great; Red Cross Still Sheltering 7,000+, Serving Thousands of
 868 Meals. *American Red Cross*, viewed 23 August 2016, [http://www.redcross.org/news/press-release/Needs-of-People-in-](http://www.redcross.org/news/press-release/Needs-of-People-in-Louisiana-Remain-Great-Red-Cross-Still-Sheltering-7000-Serving-Thousands-of-Meals)
 869 [Louisiana-Remain-Great-Red-Cross-Still-Sheltering-7000-Serving-Thousands-of-Meals](http://www.redcross.org/news/press-release/Needs-of-People-in-Louisiana-Remain-Great-Red-Cross-Still-Sheltering-7000-Serving-Thousands-of-Meals).
- 870 Broach, D.: How many houses, people flooded in Louisiana? *NOLA*, viewed 24 August 2016,
 871 http://www.nola.com/weather/index.ssf/2016/08/how_many_people_houses_were_fl.html.
- 872 Bromwich, J.E.: Flooding in the South Looks a Lot Like Climate Change, *The New York Times*, viewed 24 August 2016,
 873 <http://www.nytimes.com/2016/08/17/us/climate-change-louisiana.html>.
- 874 Burton, J. and A. Demas: Six streamgages Set peaks of record and 50 stations were overtopped by floodwaters. *USGS*,
 875 viewed 22 August 2016, <https://www.usgs.gov/news/usgs-records-historic-flooding-south-louisiana>.
- 876 Centre for Research on the Epidemiology of Disasters (CRED): The Human Cost of Natural Disasters 2015, A Global
 877 Perspective; ReliefWeb, viewed on 29 August 2016 http://reliefweb.int/sites/reliefweb.int/files/resources/PAND_report.pdf
- 878 Chen, C.-T., and Knutson, T.: On the verification and comparison of extreme rainfall indices from climate models. *J.*
 879 *Climate*, 21 (7), 1605–1621, 2008.
- 880 Christidis, N., Stott, P.A., Scaife, A.A., Arribas, A., Jones, G.S., Copsey, D., Knight, J.R. and Tennant, W.J.: A new
 881 HadGEM3-A-based system for attribution of weather-and climate-related extreme events. *J. Climate*, 26(9), pp.2756-2783,
 882 2013.
- 883 Collins, M., Knutti, R., Arblaster, J., Dufresne, J.-L., Fichet, T., Friedlingstein, P., Gao, X., Gutowski, W.J., Johns, T.,
 884 Krinner, G., Shongwe, M., Tebaldi, C., Weaver, A.J., and Wehner, M.: Long-term Climate Change: Projections,
 885 Commitments and Irreversibility. In *Climate Change 2013: The Physical Science Basis, Contribution of Working Group I to*
 886 *the Fifth Assessment Report of the Intergovernmental Panel on Climate Change*. [Stocker, T.F., Qin, D., Plattner, G.-K.,
 887 Tignor, M., Allen, S.K., Boschung, J., Nauels, A., Xia, Y., Bex, V., and Midgley, P.M. (eds.)]. Cambridge University Press,
 888 Cambridge, United Kingdom and New York, NY, USA. 2013.
- 889 Coles, S.: *An Introduction to Statistical Modeling of Extreme Values*, Springer Series in Statistics, London, UK, 2001.
- 890 Cutlip, K 2013, 'Weather Front', *Weatherwise*, 66, 2, p. 6, MAS Ultra - School Edition, EBSCOhost, viewed 29 August
 891 2016.
- 892 Dai, A.: Precipitation characteristics in eighteen coupled climate models. *J. Climate*, 19(18), 4605-4630, 2006.
- 893 Davies, R.: Louisiana Rivers at Record Levels, President Declares Major Disaster. *Floodlist*, viewed 23 August 2016,
 894 <http://floodlist.com/america/usa/usa-louisiana-rivers-record-levels-president-declares-major-disaster>.
- 895 Delworth, T.L., Broccoli, A.J., Rosati, A., Stouffer, R.J., Balaji, V., Beesley, J.A., Cooke, W.F., Dixon, K.W., Dunne, J.,
 896 Dunne, K.A. and Durachta, J.W., Findell, K., Ginoux, P., Gnanadesikan, A., Gordon, C.T., Griffies, S., Gudgel, R., Harrison,
 897 M., Held, I., Hemler, R., Horowitz, L., Klein, S., Knutson, T., Kushner, P., Langenhorst, A., Lee, H.-C., Lin, S.-J., Lu, J.,
 898 Malyshev, S., Milly, P.C.D., Ramaswamy, V., Russell, J., Schwarzkopf, M.D., Shevliakova, E., Sirutis, j., Spelman, M.,
 899 Stern, W., Winton, M., Wittenberg, A., Wyman, B., Zeng, F., Zhang, R.: GFDL's CM2 global coupled climate models. Part
 900 I: Formulation and simulation characteristics. *J. Climate*, 19(5), 643-674, 2006.
- 901 Delworth, T.L., Rosati, A., Anderson, W., Adcroft, A.J., Balaji, V., Benson, R., Dixon, K., Griffies, S.M., Lee, H.C.,
 902 Pacanowski, R.C., Vecchi, G.A., Wittenberg, A.T., Zeng, F., and Zhang, R.: Simulated climate and climate change in the
 903 GFDL CM2. 5 high-resolution coupled climate model. *J. Climate*, 25(8), 2755-2781, 2012.



- 904 Delworth, T.L., Zeng, F., Rosati, A., Vecchi, G.A. and Wittenberg, A.T.: A link between the hiatus in global warming and
905 North American drought. *J. Climate*, 28(9), 3834–3845, 2015.
- 906 Eggert, B., Berg, P., Haerter, J.O., Jacob, D. and Moseley, C.: Temporal and spatial scaling impacts on extreme
907 precipitation. *Atmospheric Chemistry and Physics*, 15(10), 5957–5971, 2015.
- 908 Emanuel, K., and Sobel, A.: Response of tropical sea surface temperature, precipitation, and tropical cyclone-related
909 variables to changes in global and local forcing. *J. of Advances in Modeling Earth Systems*, doi:10.1002/jame.20032, 2013.
- 910 Emanuel, K., Solomon, S., Folini, D., Davis, S., and Cagnano, C.: Influence of Tropical Tropopause Layer Cooling on
911 Atlantic Hurricane Activity. *J. Climate*, doi:10.1175/JCLI-D-12-00242.1, 2013
- 912 FEMA: Federal Support for Louisiana Continues, \$127 Million in Financial Assistance Provided to Louisiana Flood
913 Survivors So Far. FEMA, viewed 23 August 2016, <<https://www.fema.gov/news-release/2016/08/23/federal-support-louisiana-continues-127-million-financial-assistance>>
- 914
- 915 Flato, G., Marotzke, J., Abiodun, B., Braconnot, P., Chou, S.C., Collins, W.J., Cox, P., Driouech, F., Emori, S., Eyring,
916 V. and Forest, C., Gleckler, P., Guilyardi, E., Jakob, C., Kattsov, V., Reason, C., Rummukainen, M.: *Evaluation of
917 Climate Models. In: Climate Change 2013: The Physical Science Basis. Contribution of Working Group I to the Fifth
918 Assessment Report of the Intergovernmental Panel on Climate Change.* Climate Change 2013, 5,741–866, 2013.
- 919 Forster, P. M., T. Andrews, P. Good, J. M. Gregory, L. S. Jackson, and M. Zelinka: Evaluating adjusted forcing and
920 model spread for historical and future scenarios in the CMIP5 generation of climate models, *J. Geophys. Res. Atmos.*,
921 118, 1139–1150, doi:10.1002/jgrd.50174, 2013.
- 922 Gandin, L. S., and R. Hardin: *Objective analysis of meteorological fields*, Vol. 242. Israel program for scientific translations
923 Jerusalem, 1965.
- 924 GISTEMP Team: GISS Surface Temperature Analysis (GISTEMP). NASA Goddard Institute for Space Studies. Dataset
925 accessed 2016-08-08 at <<http://data.giss.nasa.gov/gistemp/>>.
- 926 Haarsma, R. J., Roberts, M., Vidale, P. L., Senior, C. A., Bellucci, A., Bao, Q., Chang, P., Corti, S., Fučkar, N. S.,
927 Guemas, V., von Hardenberg, J., Hazeleger, W., Kodama, C., Koenigk, T., Leung, L. R., Lu, J., Luo, J.-J., Mao, J.,
928 Mizielinski, M. S., Mizuta, R., Nobre, P., Satoh, M., Scoccimarro, E., Semmler, T., Small, J., and von Storch, J.-S.:
929 High Resolution Model Intercomparison Project (HighResMIP), *Geosci. Model Dev. Discuss.*, doi:10.5194/gmd-2016-
930 66, in review, 2016.
- 931 Hansen, J., Ruedy, R., Sato, M. and Lo, K.: Global surface temperature change. *Reviews of Geophysics*, 48(4), 2010.
- 932 Harris, L.M, Lin, S.-J., and Tu, C.Y.: High resolution climate simulations using GFDL HiRAM with a stretched global grid.
933 *J. Climate*, 29, 4293–4314, 2016.
- 934 Hawkins, E. and Sutton, R.: The potential to narrow uncertainty in regional climate predictions. *Bulletin of the American
935 Meteorological Society*, 90(8), 1095, 2009.
- 936 Hazeleger, W. Wang, X., Severijns, C., Stefanescu, S., Bintanja, R., Sterl, A., Wyser, K., Semmler, T., Yang, S., Van den
937 Hurk, B., Van Noije, T., Van der Linden, E., Van der Wiel, K.: EC-Earth V2.2: description and validation of a new seamless
938 earth system prediction model. *Clim.Dyn.*, 39, 2611–2629, 2012.
- 939 Hazeleger, W., Wouters, B., Oldenborgh, G.J., Corti, S., Palmer, T., Smith, D., Dunstone, N., Kröger, J., Pohlmann, H. and
940 Storch, J.S.: Predicting multiyear north atlantic ocean variability. *Journal of Geophysical Research: Oceans*, 118(3), 1087-
941 1098, 2013.



- 942 Herscher, R.: “Flooding in Louisiana Raises Questions About Timing, Urgency of Warnings” *NPR*, viewed 29 August 2016,
943 <[http://www.npr.org/sections/thetwo-way/2016/08/22/490916070/flooding-in-louisiana-raises-questions-about-timing-](http://www.npr.org/sections/thetwo-way/2016/08/22/490916070/flooding-in-louisiana-raises-questions-about-timing-urgency-of-warnings)
944 [urgency-of-warnings](http://www.npr.org/sections/thetwo-way/2016/08/22/490916070/flooding-in-louisiana-raises-questions-about-timing-urgency-of-warnings)>.
- 945 Higgins, R. W., W. Shi, E. Yarosh, and R. Joyce: Improved United States precipitation quality control system and analysis.
946 NOAA, National Weather Service, National Centers for Environmental Prediction, *Climate Prediction Center Atlas*, 2000.
- 947 Huang, B., Banzon, V.F., Freeman, E., Lawrimore, J., Liu, W., Peterson, T.C., Smith, T.M., Thorne, P.W., Woodruff, S.D.
948 and Zhang, H.M.: Extended reconstructed sea surface temperature version 4 (ERSST. v4). Part I: upgrades and
949 intercomparisons. *J. Climate*, 28(3), 911-930, 2015.
- 950 Jia, L., Yang, X., Vecchi, G.A., Gudgel, R.G., Delworth, T.L., Rosati, A., Stern, W.F., Wittenberg, A.T., Krishnamurthy, L.,
951 Zhang, S. and Msadek, R.: Improved seasonal prediction of temperature and precipitation over land in a high-resolution
952 GFDL climate model. *J. Climate*, 28(5), 2044-2062, 2015.
- 953 Jia, L., Vecchi, G.A., Yang, X., Gudgel, R., Delworth, T., Stern, W., Paffendorf, K., Underwood, S., Zeng, F.: The Roles of
954 Radiative Forcing, Sea Surface Temperatures, and Atmospheric and Land Initial Conditions in U.S. Summer Warming
955 Episodes. *J. Climate*, doi:10.1175/JCLI-D-15-0471.1, 2016.
- 956 Kalnay, E., Kanamitsu, M., Kistler, R., Collins, W., Deaven, D., Gandin, L., Iredell, M., Saha, S., White, G., Woollen, J. and
957 Zhu, Y.: The NCEP/NCAR 40-year reanalysis project. *Bulletin of the American meteorological Society*, 77(3), 437-471,
958 1996.
- 959 Katsman, C.A., Hazeleger, W., Drijfhout, S.S., van Oldenborgh, G.J. and Burgers, G.: Climate scenarios of sea level rise for
960 the northeast Atlantic Ocean: a study including the effects of ocean dynamics and gravity changes induced by ice melt.
961 *Climatic Change*, 91(3-4), 351-374, 2008.
- 962 Keim, B.D. and Faiers, G.E.: Heavy rainfall distributions by season in Louisiana: Synoptic interpretations and quantile
963 estimates. *Water Resources Bulletin*, 32(1), 117-124, 1996.
- 964 Kirtman, B., Power, S.B., Adedoyin, J.A., Boer, G.J., Bojariu, R., Camilloni, I., Doblas-Reyes, F.J., Fiore, A.M., Kimoto,
965 M., Meehl, G.A., Prather, M., Sarr, A., Schär, C., Sutton, R., Van Oldenborgh, G.J., Vecchi, G., and Wang, H.-J.: Near-term
966 climate change: projections and predictability. In *Climate Change 2013: The Physical Science Basis, Contribution of*
967 *Working Group I to the Fifth Assessment Report of the Intergovernmental Panel on Climate Change*. [Stocker, T.F., Qin, D.,
968 Plattner, G.-K., Tignor, M., Allen, S.K., Boschung, J., Nauels, A., Xia, Y., Bex, V., and Midgley, P.M. (eds.)]. Cambridge
969 University Press, Cambridge, United Kingdom and New York, NY, USA. 2013.
- 970 Knapp, K.R., Kruk, M.C., Levinson, D.H., Diamond, H.J. and Neumann, C.J.: The international best track archive for
971 climate stewardship (IBTrACS). *Bulletin of the American Meteorological Society*, 91(3), 363, 2010.
- 972 Knutson, T.R., Sirutis, J.J., Vecchi, G.A., Garner, S., Zhao, M., Kim, H.S., Bender, M., Tuleya, R.E., Held, I.M. and
973 Villarini, G.: Dynamical downscaling projections of twenty-first-century Atlantic hurricane activity: CMIP3 and CMIP5
974 model-based scenarios. *J. Climate*, 26(17), 6591-6617, 2013.
- 975 Krishnamurthy, L., Vecchi, G., Msadek, R., Wittenberg, A., Delworth, T., and Zeng, F.: The Seasonality of the Great Plains
976 Low-Level Jet and ENSO Relationship. *J. Climate*. doi:10.1175/JCLI-D-14-00590.1, 2015.
- 977 Lehmann, J., Coumou, D. and Frieler, K.: Increased record breaking precipitation events under global warming. *Climatic*
978 *Change*, 132(4), 501-505, doi:10.1007/s10584-015-1434-y, 2015.
- 979 Lenderink, G. and Attema, J.: A simple scaling approach to produce climate scenarios of local precipitation extremes for the
980 Netherlands. *Environmental Research Letters*, 10(8), 085001, 2015.
- 981 Little, C.M., Horton, R.M., Kopp, R.E., Oppenheimer, M., Vecchi, G.A., and Villarini, G.: Joint projections of US East
982 Coast sea level and storm surge. *Nature Climate Change*. doi:10.1038/nclimate2801, 2015.



- 983 Lin, N., Emanuel, K., Oppenheimer, M. and Vanmarcke, E.: Physically based assessment of hurricane surge threat under
984 climate change. *Nature Climate Change*, 2(6), 462-467, 2012.
- 985 Lin, N., Lane, P., Emanuel, K.A., Sullivan, R.M., and Donnelly, J.P.: Heightened hurricane surge risk in northwest Florida
986 revealed from climatological-hydrodynamic modeling and paleorecord reconstruction. *J. Geophys. Res. (Atmospheres)*,
987 doi:10.1002/2014JD021584, 2014
- 988 Massey, N., Jones, R., Otto, F.E.L., Aina, T., Wilson, S., Murphy, J.M., Hassell, D., Yamazaki, Y.H., and M.R. Allen:
989 weather@home - development and validation of a very large ensemble modelling system for probabilistic event attribution.
990 *Q. J. Royal Met. Soc.*, doi:10.1002/qj.2455, 2015.
- 991 Menne, M.J., I. Durre, R.S. Vose, B.E. Gleason, and T.G. Houston: An overview of the Global Historical Climatology
992 Network-Daily Database. *Journal of Atmospheric and Oceanic Technology*, 29, 897-910, 2012.
993
- 994 Menne, M.J., I. Durre, B. Korzeniewski, S. McNeal, K. Thomas, X. Yin, S. Anthony, R. Ray, R.S. Vose, B.E. Gleason, and
995 T.G. Houston: Global Historical Climatology Network-Daily (GHCN-Daily), Version 3.22. *NOAA National Climatic Data*
996 *Center*. <http://doi.org/10.7289/V5D21VHZ> 19 August 2016.
- 997 De Michele, C. and Salvadori, G.: On the derived flood frequency distribution: analytical formulation and the influence of
998 antecedent soil moisture condition. *Journal of Hydrology*, 262(1), 245-258, 2002.
- 999 Milman, O.: Disasters like Louisiana floods will worsen as planet warms, scientists warn, *The Guardian*, viewed 24 August
000 2016, <[https://www.theguardian.com/environment/2016/aug/16/louisiana-flooding-natural-disaster-weather-climate-](https://www.theguardian.com/environment/2016/aug/16/louisiana-flooding-natural-disaster-weather-climate-change)
001 [change](https://www.theguardian.com/environment/2016/aug/16/louisiana-flooding-natural-disaster-weather-climate-change)>.
- 002 Moftakhari, H.R., AghaKouchak, A., Sanders, B.F., Feldman, D.L., Sweet, W., Matthew, R.A. and Luke, A.: Increased
003 nuisance flooding along the coasts of the United States due to sea level rise: Past and future. *Geophys. Res. Lett.*, 42(22),
004 2015.
- 005 Msadek, R., Vecchi, G.A., Winton, M., Gudgel, R.: Importance of initial conditions in seasonal predictions of Arctic sea ice
006 extent. *Geophys. Res. Lett.*, DOI: 10.1002/2014GL060799, 2014.
- 007 Murakami, H., and Wang, B.: Future Change of North Atlantic Tropical Cyclone Tracks: Projection by a 20-km-Mesh
008 Global Atmospheric Model. *J. Climate*, doi:10.1175/2010JCLI3338.1, 2010.
- 009 Murakami, H., Vecchi, G.A., Underwood, S., Delworth, T., Wittenberg, A.T., Anderson, W., Chen, J.-H., Gudgel, R., Harris,
010 L., Lin, S.-J., and Zeng, F.: Simulation and prediction of Category 4 and 5 hurricanes in the high-resolution GFDL HiFLOR
011 coupled climate model. *J. Climate*, doi:10.1175/JCLI-D-15-0216.1, 2015.
- 012 Murakami, H., Vecchi, G.A., Villarini, G., Delworth, T., Gudgel, R., Underwood, S.D., Yang, X., Zhang, W., Lin, S.-J.:
013 Seasonal Forecasts of Major Hurricanes and Landfalling Tropical Cyclones using a High-Resolution GFDL Coupled Climate
014 Model. *J. Climate*, 10.1175/JCLI-D-16-0233.1, 2016.
- 015 National Weather Service: Southern and Eastern U.S. Heavy Rainfall, storm summaries 1-19, viewed 23 August 2016,
016 <http://www.wpc.ncep.noaa.gov/winter_storm_summaries/storm15/storm15_archive.shtml> and New Orleans area forecast
017 discussions (PIL=AFDLIX), viewed 24 August 2016, <<https://mesonet.agron.iastate.edu/wx/afos/>>.
- 018 O’Gorman, P.A.: Precipitation extremes under climate change. *Current climate change reports*, 1(2), 49-59, 2015.
- 019 Otto, F.E., Van Oldenborgh, G.J., Eden, J., Stott, P.A., Karoly, D.J. and Allen, M.R.: The attribution question. *Nature*
020 *Climate Change*, 6(9), pp.813-816, 2016.
- 021 Pascale, S., Bordoni, S., Kapnick, S.B., Vecchi, G.A., Jia, L., Delworth, T.L., Underwood, S. Anderson, W.: The impact of
022 horizontal resolution on North American monsoon Gulf of California moisture surges in a suite of coupled global climate
023 models. *J. Climate*, doi:10.1175/JCLI-D-16-0199.1, 2016.



- 024 Pinter, N., van der Ploeg, R.R., Schweigert, P. and Hoefler, G.: Flood magnification on the River Rhine. *Hydrological*
025 *Processes*, 20(1), 147-164, 2006.
- 026 Putman, W. M., and S.-J. Lin: Finite-volume transport on various cubed-sphere grids. *Journal of Computational Physics*,
027 227 (1), 55–78, 2007.
- 028 Rantz, S.E.: Measurement and computation of streamflow: volume 2, computation of discharge (No. 2175). USGPO, 1982.
029 Available at: <http://pubs.usgs.gov/wsp/wsp2175/pdf/WSP2175_voll1a.pdf>.
- 030 Rayner, N.A., Parker, D.E., Horton, E.B., Folland, C.K., Alexander, L.V., Rowell, D.P., Kent, E.C. and Kaplan, A.: Global
031 analyses of sea surface temperature, sea ice, and night marine air temperature since the late nineteenth century. *Journal of*
032 *Geophysical Research: Atmospheres*, 108(D14), doi:10.1029/2002JD002670, 2003.
- 033 Stafford, Robert, T., Stafford disaster relief and emergency assistance act. *Public Law*, 10(30), 106-390, 2000.
- 034 Scherrer, S.C., Fischer, E.M., Posselt, R., Liniger, M.A., Croci-Maspoli, M. and Knutti, R.: Emerging trends in heavy
035 precipitation and hot temperature extremes in Switzerland. *Journal of Geophysical Research: Atmospheres*,
036 doi:10.1002/2015JD024634, 2016.
- 037 Schleifstein, M.: Louisiana Flood of 2016 resulted from '1,000-year' rain in 2 days, *NOLA*, viewed at 23 August 2016,
038 <http://www.nola.com/weather/index.ssf/2016/08/louisiana_flood_of_2016_result.html>.
- 039 Sterl, A., Brink, H.V.D., Vries, H.D., Haarsma, R. and Meijgaard, E.V.: An ensemble study of extreme storm surge related
040 water levels in the North Sea in a changing climate. *Ocean Science*, 5(3), 369-378, 2009.
- 041 Strum, B.: Damage Grows from Louisiana Flood. *Wall Street Journal*, viewed at 23 August 2016,
042 <<http://www.wsj.com/articles/damage-grows-from-louisiana-flood-1471803140>>.
- 043 Taylor, K.E., Stouffer, R.J. and Meehl, G.A.: An overview of CMIP5 and the experiment design. *Bulletin of the American*
044 *Meteorological Society*, 93(4), 485-498, 2012.
- 045 Trambly, Y., Bouvier, C., Martin, C., Didon-Lescot, J.F., Todorovik, D. and Domergue, J.M.: Assessment of initial soil
046 moisture conditions for event-based rainfall–runoff modelling. *Journal of Hydrology*, 387(3), 176-187, 2010.
- 047 Van der Wiel, K., Kapnick S.B., Vecchi G.A., Cooke, W.F., Delworth T.L., Jia L., Murakami H., Underwood S., and Zeng
048 F.: The resolution dependence of contiguous US precipitation extremes in response to CO2 forcing. *J. Climate*, doi:
049 10.1175/JCLI-D-16-0307.1, 2016.
- 050 Van Oldenborgh, G. J., Otto, F. E. L., Haustein, K., and Cullen, H.: Climate change increases the probability of heavy rains
051 like those of storm Desmond in the UK – an event attribution study in near-real time, *Hydrol. Earth Syst. Sci. Discuss.*, 12,
052 13197-13216, doi:10.5194/hessd-12-13197-2015, in review, 2015.
- 053 Van Oldenborgh, G. J., Philip, S., Aalbers, E., Vautard, R., Otto, F., Haustein, K., Habets, F., Singh, R., and Cullen, H.:
054 Rapid attribution of the May/June 2016 flood-inducing precipitation in France and Germany to climate change, *Hydrol.*
055 *Earth Syst. Sci. Discuss.*, doi:10.5194/hess-2016-308, in review, 2016.
- 056 Van Vuuren, D.P., Edmonds, J., Kainuma, M., Riahi, K., Thomson, A., Hibbard, K., Hurtt, G.C., Kram, T., Krey, V.,
057 Lamarque, J.F., Masui, T., Meinshausen, M., Nakicenovic, N., Smith, S., and Rose, S.: The representative concentration
058 pathways: an overview. *Climatic change*, 109, 5-31, 2011.
- 059 Vecchi, G.A., Fueglistaler, S., Held, I.M., Knutson, T.R., and Zhao, M.: Impacts of Atmospheric Temperature Changes on
060 Tropical Cyclone Activity. *J. Climate* doi: 10.1175/JCLI-D-12-00503.1, 2013.
- 061 Vecchi, G.A., and Soden. B.J.: Effect of remote sea surface temperature change on tropical cyclone potential intensity,
062 *Nature*, 450, 1066-1070 doi:10.1038/nature06423, 2007.



- 063 Vecchi, G.A., Delworth, T., Gudgel, R., Kapnick, S.B., Rosati, A., Wittenberg, A.T., Zeng, F., Anderson, W., Balaji, V.,
064 Dixon, K. Jia, L., Kim, H-S, Krishnamurthy, L., Msadek, R., Stern, W.F, Underwood, S.D., Villarini, G., Yang, X., and
065 Zhang, S.: On the seasonal forecasting of regional tropical cyclone activity. *J. Climate*, 27(21), 7994-8016, 2014.
- 066 Villarini, G., Goska, R., Smith, J.A. and Vecchi, G.A.: North Atlantic tropical cyclones and US flooding. *Bulletin of the*
067 *American Meteorological Society*, 95(9), 1381-1388, 2014.
- 068 Walsh, K., Camargo, S., Vecchi, G., Daloz, A., Elsner, J., Emanuel, K., Horn, M., Lim, Y.-K., Roberts, M., Patricola, C.,
069 Scoccimarro, E., Sobel, A., Strazzo, S., Villarini, G., Wehner, M., Zhao, M., Kossin, J., LaRow, T., Oouchi, K., Schubert, S.,
070 Wang, H., Bacmeister, J., Chang, P., Chauvin, F., Jablonowski, C., Kumar, A., Murakami, H., Ose, T., Reed, K., Saravanan,
071 R., Yamada, Y., Zarzycki, C., Vidale, P., Jonas, J., Henderson, N.: Hurricanes and climate: the U.S. CLIVAR working group
072 on hurricanes. *Bull. Amer. Meteorol. Soc.* doi:10.1175/BAMS-D-13-00242.1, 2015.
- 073 Yang, X., Vecchi, G.A., Gudgel, R.G., Delworth, T.L., Zhang, S., Rosati, A., Jia, L., Stern, W.F., Wittenberg, A.T.,
074 Kapnick, S. and Msadek, R.: Seasonal predictability of extratropical storm tracks in GFDL's high-resolution climate
075 prediction model. *J. Climate*, 28(9), 3592-3611, 2015.
- 076 Zhang, W., Vecchi, G.A., Murakami, H., Delworth, T., Wittenberg, A.T., Anderson, W., Rosati, A., Underwood, S., Harris,
077 L., Gudgel, R., Lin, S.-J., Villarini, G., and Chen, J.-H.: Improved Simulation of Tropical Cyclone Responses to ENSO in
078 the Western North Pacific in the High-Resolution GFDL HiFLOR Coupled Climate Model. *J. Climate*, doi:10.1175/JCLI-D-
079 15-0475.1, 2016.
- 080 Zhang, W., Leung, Y. and Fraedrich, K.: Different El Niño types and intense typhoons in the Western North Pacific. *Climate*
081 *Dynamics*, 44(11-12), 2965-2977, 2015.